

Ligand binding to a remote site thermodynamically corrects the F508del mutation  
in the human cystic fibrosis transmembrane conductance regulator

**Authors:** Chi Wang<sup>1</sup>, Andrei A. Aleksandrov<sup>2†</sup>, Zhengrong Yang<sup>3†</sup>, Farhad Forouhar<sup>1§</sup>, Elizabeth A. Proctor<sup>2§</sup>, Pradeep Kota<sup>2§</sup>, Jianli An<sup>3</sup>, Anna Kaplan<sup>1</sup>, Netaly Khazanov<sup>4</sup>, Grégory Boël<sup>1§</sup>, Brent R. Stockwell<sup>1,5</sup>, Hanoch Senderowitz<sup>4</sup>, Nikolay V. Dokholyan<sup>2</sup>, John R. Riordan<sup>2</sup>, Christie G. Brouillette<sup>3</sup>, John F. Hunt<sup>1\*</sup>

**Affiliations:** <sup>1</sup>Department of Biological Sciences, Columbia University, New York, NY 10027, USA; <sup>2</sup>Department of Biochemistry and Biophysics, School of Medicine, University of North Carolina, Chapel Hill, NC 27599, USA; <sup>3</sup>Department of Chemistry, University of Alabama, Birmingham, AL 35294, USA; <sup>4</sup>Department of Chemistry, Bar-Ilan University, Ramat-Gan, 5290002, Israel; <sup>5</sup>Department of Chemistry, Columbia University, New York, NY 10027, USA.

**Running Title:** *Thermodynamic correction of F508del-CFTR*

† Authors who contributed equally

\*To whom correspondence should be addressed: Professor John F. Hunt Department of Biological Sciences, Columbia University, New York, NY 10027 (212)-854-5443voice; (212)-865-8246FAX; E-mail: jfh21@columbia.edu.

**Keywords:** cystic fibrosis; CFTR; F508del mutation; protein thermodynamics; protein aggregation; fluorescence resonance energy transfer; high-throughput screening; calorimetry; single-channel electrophysiology; isothermal titration calorimetry (ITC); deoxythymidine.

## Abstract

Many disease-causing mutations impair protein stability. Here, we explore a thermodynamic strategy to correct the disease-causing F508del mutation in the human cystic fibrosis transmembrane conductance regulator (hCFTR). F508del destabilizes nucleotide-binding domain 1 (hNBD1) in hCFTR relative to an aggregation-prone intermediate. We developed a fluorescence self-quenching assay for compounds that prevent aggregation of hNBD1 by stabilizing its native conformation. Unexpectedly, we found that dTTP and nucleotide analogs with exocyclic methyl groups bind to hNBD1 more strongly than ATP and preserve electrophysiological function of full-length F508del-hCFTR channels at temperatures up to 37 °C. Furthermore, nucleotides that increase open-channel probability, which reflects stabilization of an interdomain interface to hNBD1, thermally protect full-length F508del-hCFTR even when they do not stabilize isolated hNBD1. Therefore, stabilization of hNBD1 itself or of one of its interdomain interfaces by a small molecule indirectly offsets the destabilizing effect of the F508del mutation on full-length hCFTR. These

results indicate that high-affinity binding of a small molecule to a remote site can correct a disease-causing mutation. We propose that the strategies described here should be applicable to identifying small molecules to help manage other human diseases caused by mutations that destabilize native protein conformation.

## Introduction

Cystic fibrosis (CF) is the most frequent lethal genetic disease afflicting Caucasians and is common in some other human populations (1). It causes pervasive defects in secretory processes, including water secretion in the lungs (2). This defect leads to insufficient hydration of the lung epithelium, which impairs bacterial clearance and leads to persistent cycles of infection/inflammation that ends in lung failure. CF is caused by mutations (3) in the human Cystic Fibrosis Transmembrane Conductance Regulator (hCFTR), a protein belonging to the ATP-binding cassette (ABC) superfamily (4-12) that functions as an ATP-dependent chloride ion channel in epithelial tissues (13,14). The most common disease-causing mutation in hCFTR is in-frame deletion of

phenylalanine 508 (F508del) (1,15), located in the  $\alpha$ -helical (ABC $\alpha$ ) subdomain of nucleotide-binding domain 1 (NBD1) (9,16-18). Based on a cryo-EM structure of hCFTR (19) as well as homology models (20-23), F508 packs in the interface between NBD1 and the transmembrane domains (TMDs) of hCFTR, as schematized in **Figure 1**. The F508del mutation causes degradation of hCFTR by cellular quality-control systems before being transported or 'trafficked' to the site of function in the plasma membrane on the cell surface (24-26).

Previously, we demonstrated that the F508del mutation destabilizes the native conformation of isolated human NBD1 (hNBD1) (10,11) relative to a partially unfolded molten-globule conformation that aggregates aggressively *in vitro* (20,27-31). This aggregation reaction is irreversible, and computational modeling of scan-rate-dependent differential scanning calorimetry (DSC) data indicated that it is controlled by a unimolecular conformational transition within the molten globule (10). Mg-ATP binds to native hNBD1 with sub-micro molar affinity, stabilizing it relative to this aggregation-prone molten globule (**Figure 1**). Second-site mutations in hNBD1 that suppress defective trafficking of F508del-hCFTR *in vivo* also stabilize the native conformation of hNBD1 relative to the molten-globule *in vitro* (32-35), indicating that thermodynamic destabilization of hNBD1 by the F508del mutation is an important contributor to its molecular pathology. Similarly, the cosmotropic (structure-stabilizing) compound glycerol, which suppresses the trafficking defect in F508del-hCFTR *in vivo* (29,36), also stabilizes the native conformation of hNBD1 relative to the molten-globule *in vitro* (10,11,17,37). These analyses and others indicate that increasing the stability of the native conformation hNBD1 should counteract the pathological effect of the F508del mutation in hCFTR (**Figure 1**). Thermodynamic principles suggest that the binding energy of any molecular species that interacts with hNBD1 should increase its stability (38) (**Figure 1**). Therefore, tight binding of a small molecule to hNBD1 should also be able to correct the 'trafficking' defect of F508del-hCFTR, even if it binds at a remote location from the mutation site. Promoting more stable interaction of hNBD1 with other domains within hCFTR should also, in theory, correct the

trafficking defect (27,29,30,39-41).

In this paper, we demonstrate that some nucleotide analogs, which bind  $\sim 20$  Å from the site of the F508del mutation, bind to hNBD1 more tightly than the physiological ligand ATP and significantly enhance its thermal stability as well as that of full-length F508del-hCFTR. These analogs were identified using a new high-throughput screen for NBD1-stabilizing agents that we developed based on our previous biophysical studies showing that aggressive aggregation of NBD1 follows unfolding *in vitro*. This highly efficient screen detects aggregation and thereby unfolding via self-quenching of a visible fluorophore that binds at a single site in an engineered variant of hNBD1. The most strongly stabilizing nucleotides identified in this screen represent the first small molecules demonstrated to thermally stabilize significantly full-length human F508del-hCFTR. The thermodynamic approach and biophysical methods presented in this paper should be applicable to identifying small molecules as lead compounds for the treatment of other human genetic diseases caused by mutations that destabilize native protein conformation.

## Results

*Development of a fluorescence self-quenching (FSQ) assay for hNBD1 stability.* The molecular pathology caused by the F508del mutation (42) in hCFTR is attributable at least in part to destabilization of hNBD1 relative to a molten globule folding intermediate (10,11). We were then motivated to develop a sensitive and efficient assay for use in high-throughput screening for hCFTR-stabilizing compounds. Because current assays for stability of the aggregation-prone protein are technically complex, making them artefact-prone and/or difficult to adapt to high-throughput format, we sought to develop an assay that monitors aggregation of the molten globule intermediate of hNBD1, which we previously demonstrated to be tightly coupled to unfolding of native hNBD1 (10,11). Fluorescence self-quenching, which strongly attenuates emission upon oligomerization of many fluorophores (43), offered a promising approach for development of an hNBD1 unfolding/aggregation assay. The fluorescence self-quenching is caused by resonance-energy transfer between overlapping electronic absorption modes

that have different fluorescent quantum yields, and it can monitor aggregation most efficiently when each molecule bears a single fluorophore before aggregation. Therefore, we sought to initially develop an hNBD1 construct with native-like stability harboring a single cysteine residue with high reactivity towards fluorescent maleimide reagents.

A previously characterized hNBD1 construct (10,11,44) that spans residues 488-646 in hCFTR was selected because it is well behaved biochemically and biophysically (**Figure 2A**). This construct harbors an internal deletion of the regulatory insertion (RI) motif (residues 403-436) but otherwise has the native sequence of hCFTR with Met at the polymorphic site at residue 470. This construct was named hNBD1 $\Delta$ (RI,RE) in previous studies (10,11,44), but we have simplified its name to hNBD1 $\Delta$ RI in the current paper. The hNBD1 $\Delta$ RI includes four endogenous cysteine residues present in hNBD1 in wild-type hCFTR – C491, C524, C590, and C592 (**Figure 2A**). The parental protein construct was thermodynamically destabilized and aggregated upon reaction at roughly 1:1 stoichiometry with Alexa Fluor 546 (AF546) maleimide (**Figure S1B**). Therefore, we engineered hNBD1 $\Delta$ RI to remove endogenous reactive Cys residues and add a highly reactive non-native cysteine after the last residue at its C-terminus (**Figures 2 & S1**), which creates the equivalent of a G646C mutation in the native human sequence. We performed free energy calculations using Eris (45) to predict the change in the thermodynamic stability upon mutation of each or all of the endogenous Cys residues. Calculated stability correlated well with experimentally measured stability by differential scanning calorimetry (DSC) for 11 different single or multiple point mutants (**Figure 2B**). The only construct retaining native-like thermodynamic stability in this study was the C592L single mutation (**Figures 2B & C**). Because C592 is the only solvent-exposed Cys residue in hNBD1, we tried to optimize labeling conditions for the C592L/G646C-hNBD1 $\Delta$ RI construct to obtain covalent attachment of AF546 exclusively to the engineered C-terminal Cys residue (**Figures S1C & D**). We identified conditions that consistently yield incorporation of 0.80-0.90 molecules of AF546 per

C592L/G646C-hNBD1 $\Delta$ RI protomer. The resulting AF546-labeled protein preparation remains monodisperse as assayed by gel filtration chromatography (**Figure S1D**) and has a similar thermodynamic stability to the corresponding unlabeled parental construct, both when retaining the native F508 residue and when harboring the disease-causing F508del mutation (**Figure 2C**).

Triple spectroscopic detection experiments demonstrated that AF546-F508-C592L/G646C-hNBD1 $\Delta$ RI has very similar biophysical properties to the unlabeled parental domain and that self-quenching of AF546 fluorescence provides an accurate and sensitive monitor of the tightly coupled unfolding and aggregation of the domain (**Figure 3A**). These experiments were conducted as previously described (11) except for monitoring the visible fluorescence of the covalently attached AF546 dye instead of intrinsic tryptophan fluorescence. Circular dichroism (CD) spectroscopy was used to monitor protein secondary structure (top panel in **Figure 3A**), and static light-scattering (SLS) was used to measure mass-averaged particle size during isothermal chemical denaturation (**Figure S2A**) or thermal denaturation of the AF546-labeled protein (middle panel in **Figure 3A**). The fluorescence emission of AF546, which was monitored at 573 nm using 556 nm light for excitation, shows complete quenching (bottom panel in **Figure 3A**) during thermal denaturation closely coincident with the aggregation of the domain as monitored by SLS (middle panel in **Figure 3A**). The midpoint of the fluorescence self-quenching transition ( $T_{SQ}$ ) coincides with that of the SLS transition when thermal denaturation is conducted at either 30  $\mu$ M or 430  $\mu$ M Mg-ATP. The  $\sim 3.5$   $^{\circ}$ C increase in  $T_{SQ}$  in the presence of the higher concentration of Mg-ATP demonstrates the efficacy of the assay in detecting a thermodynamic stabilization of the domain by a small-molecule ligand, in this case, a natural physiological ligand. Mg-ATP stabilizes the domain because it binds to the native conformation with 200 nM affinity but has negligible affinity for the rapidly aggregating molten globule intermediate state produced by denaturation (10,11). This kind of protein folding intermediate loses the native tertiary structure but retains most of its secondary structure. Previous studies demonstrated that the rapid aggregation of the

molten globule intermediate of hNBD1 increases secondary structure slightly (10,11), resulting in minimal change in the observed CD when this intermediate is formed during isothermal chemical denaturation (top panels in **Figure S2A**) or thermal denaturation (top panel in **Figure 3A**). However, a strong reduction in CD magnitude is observed at higher temperatures in thermal titrations (top panel of **Figure 3A**) due to the unfolding of the molten-globule intermediate into a significantly less structured conformational state.

We evaluated the reproducibility and robustness of the thermal fluorescence self-quenching (tFSQ) assay by conducting it at different thermal scanning rates (**Figure S3A**) in the presence of increasing concentrations of Mg-ATP in 96-well or 384-well microtiter plates in real-time PCR machines (top panel in **Figure 3B** and **Figure S3**). Complete quenching of the fluorescence of AF546-F508del-C592L/G646C-hNBD1 $\Delta$ RI occurs in these thermal PCR-plate titrations (**Figure 3B**) over the same temperature range and heating-rate observed in the cuvette-based CD-SLS-FL assays (**Figure 3A**). The maximum of the first derivative of the fluorescence emission intensity as a function of temperature gives a readily automated quantitative estimate of  $T_{SQ}$  (bottom panel in **Figure 3B**). We used eight replicate assays conducted at 3  $\mu$ M or 2.003 mM Mg-ATP, which give mean  $T_{SQ}$  values of  $43.3 \pm 0.3$  and  $52.2 \pm 0.3$   $^{\circ}$ C, respectively, to calculate a Z-factor of 0.8 for the tFSQ assay. The Z-factor is widely used to assess the suitability of an assay for use in high-throughput screening (46), and assays characterized by Z-factors greater than 0.5, which corresponds to 12 standard deviations of separation between negative and positive controls, are considered to have excellent characteristics. The tFSQ assay performs similarly with a wide variety of AF546-labeled hNBD1 constructs harboring the C592L/G646C mutations, including the hNBD1 $\Delta$ RI construct harboring the F508del mutation (**Figure S3A-B**) and several constructs including both the RI and RE segments (**Figure S3C-E**). The performance of the tFSQ assay is unchanged in the presence of the non-ionic detergent C12E8 (**Figure 3C**), suggesting that it could be applied directly to full-length hCFTR labeled by a single visible fluorophore. Therefore, the sensitive and efficient tFSQ assay that we have

developed is applicable to high-throughput screening for compounds stabilizing a wide variety of protein constructs containing hNBD1, including in principle full-length hCFTR.

*Mg-dTTP stabilizes hNBD1 more strongly than the physiological ligand Mg-ATP.* To explore more thoroughly the characteristics of the tFSQ assay and its efficacy in detecting stabilizing ligands, we used it to evaluate the influence of the eight major physiological nucleotides on the thermal unfolding/aggregation of AF546-F508-C592L/G646C-hNBD1 $\Delta$ RI (**Figure 4A**). Whereas nucleotides bearing adenine, guanine, or uracil bases produce similar thermal stabilization and  $T_{SQ}$  values, consistent with the promiscuous nucleotide-binding properties of many ABC family ATPases (8,47), thymine-containing nucleotides produce greater thermal stabilization, as manifested by higher  $T_{SQ}$ . At a 2 mM nucleotide concentration,  $T_{SQ}$  is consistently  $\sim 2.5$   $^{\circ}$ C higher for the Mg<sup>++</sup> complex of thymine-containing nucleotides compared to adenine-containing nucleotides for all hNBD1 constructs tested, including AF546-F508-C592L/G646C-hNBD1 $\Delta$ RI (**Figure 4A**), the equivalent construct harboring the F508del mutation (**Figure S3B**), and a variety of constructs including the RI and RE segments (**Figure S3C-E**). A similar stabilizing effect for thymine compared to adenine is observed in isothermal fluorescence self-quenching (iFSQ) assays conducted in a high-throughput format (**Figure S2B**).

The convenient properties of the high-throughput tFSQ assay enabled rapid completion of an extensive structure-activity study on nucleotide interaction with hNBD1 (**Figures 4A-B & S4-S5**). Nucleotides with 14 different base structures all produce substantial stabilization of the domain compared to the control, indicating they all bind with high affinity (**Figure S5**). A variety of nucleotides with exocyclic base modifications stabilize the domain more strongly than ATP, with 7-methyl-GTP (7Me-GTP) producing the greatest stabilization among the nucleotides analyzed ( $\Delta T_{SQ} = +3.3$   $^{\circ}$ C compared to ATP and  $\Delta T_{SQ} = +1.0$   $^{\circ}$ C compared to dTTP). Addition of an exocyclic methyl group to a given base structure consistently produces an increase in  $T_{SQ}$  of  $\sim 3$   $^{\circ}$ C (*i.e.*, dTTP vs. dUTP, 7Me-GTP vs. GTP, and 5-methyl-dCTP (5Me-CTP) vs. dCTP in **Figure S5**).

Equivalent  $T_{SQ}$  values are observed for ribose and deoxyribose nucleotides bearing the same base, as well as for nucleotides harboring other modifications at the 2' and 3' positions on the ribose (**Figures 4A, S3C, & S5**). However, diphosphate nucleotides consistently give  $T_{SQ}$  values  $\sim 4$  °C lower than the corresponding triphosphate nucleotides, whereas monophosphate nucleotides produce no significant shift compared to the control (**Figure S4A**). Therefore, the monophosphates have negligible affinity for hNBD1, and the triphosphates have substantially higher binder energy than the diphosphates, at least in the temperature range of the unfolding reaction. Complete depletion of  $Mg^{++}$  reduces  $T_{SQ}$  by more than 10 °C (**Figure S4B-C**), indicating that the  $Mg^{++}$  cofactor contributes significantly to the energy of nucleotide binding to hNBD1. However, even when  $Mg^{++}$  is fully depleted, 2 mM ATP increases  $T_{SQ}$  by +1.0 °C, and 2 mM dTTP increases  $T_{SQ}$  by +3.0 °C (**Figure S4C**), indicating that the nucleotides retain significant binding affinity in the absence of the  $Mg^{++}$  cofactor, possibly reflecting its replacement by  $Na^+$  in the protein-bound state (8). The greater stabilization by dTTP compared to ATP even in the absence of  $Mg^{++}$  provides further evidence that the thymine base has higher binding energy than adenine for the native conformation of hNBD1.

*Calorimetric studies confirm the thermodynamic inferences from the tFSQ assays.* We used differential scanning calorimetry (DSC), which directly monitors unfolding of the native conformation of hNBD1 $\Delta$ RI into the molten globule state (10), to confirm that the tFSQ assay accurately reports on thermodynamic stabilization of the domain. The shift in the thermal melting temperature ( $T_m$ ) measured in DSC assays conducted in the presence of a 0.5 mM concentration of four representative nucleotides (**Figure 4C**) closely matches the shift in  $T_{SQ}$  in fluorescence self-quenching assays conducted in the presence of a 2.0 mM concentration of the same species (**Figure 4D**). These results confirm our hypothesis that tight coupling of the unfolding of hNBD1 to aggregation enables the stability of the domain to be monitored reliably by an assay detecting aggregation.

Isothermal titration calorimetry (ITC) was used to quantify the binding affinities of 11 nucleotides characterized using tFSQ assays (**Figure 4E & Table S1**). These measurements were conducted at 10° C to minimize aggregation during data collection, which starts in a nucleotide-free buffer containing the domain at  $\sim 1$  mg/ml. Consistent with the greater stabilization of hNBD1 $\Delta$ RI by dTTP compared to ATP in our tFSQ assays, ITC demonstrates that dTTP binds to hNBD1 with  $\sim 2.3$ -fold higher affinity than ATP ( $98 \pm 26$  nM vs.  $228 \pm 32$  nM) (Table S1), corresponding to  $\Delta\Delta G_{dTTP-ATP}$  of -0.47 kcal/mol. The substantial increase in thermal stability produced by a small improvement in binding energy reflects the physical and thermodynamic complexities of the thermal unfolding reaction, which involves a very steep change in protein stability over a narrow temperature range. For most proteins, the stability of the native conformation relative to their unfolded state is determined by a small difference between large and offsetting enthalpy and entropy differences that vary substantially with temperature due primarily to changes in solvent dynamics. The complex thermodynamic processes controlling thermal unfolding enable relatively small energetic differences between the native and unfolded states to produce large changes in thermal stability. Because nucleotides bind tightly to the native conformation of hNBD1 but not significantly to the molten globule intermediate produced by thermal denaturation (10,11), their binding energy directly adds to the stability of the native conformation. The thermodynamic results showing that a -0.47 kcal/mol change in binding free energy produces a 2.5 °C increase in thermal stability (**Figure 4**) suggests that modest improvements in ligand-binding affinity should be able to offset the full 7 °C change in the thermal stability of hNBD1 produced by the F508del mutation.

The ITC data demonstrate that all 11 nucleotides bind to hNBD1 $\Delta$ RI with favorable enthalpy, reflecting a net gain in electrostatic and van der Waals interactions, but unfavorable entropy, reflecting a loss in motional freedom in the ligand and possibly the protein. Comparing the ITC data on dTTP and dUTP shows that the exocyclic methyl group at the 5 position on the pyrimidine base in dTTP, which is the only difference compared to

dUTP, increases the entropy of binding to hNBD1ΔRI by +5.0 cal/mol/°C (top of lower section in **Table S1**). This effect increases the magnitude of Gibbs Free Energy of binding by 1.4 kcal/mol, but an offsetting 0.3 kcal/mol reduction in the magnitude of the enthalpy of binding decreases the net gain in the Gibbs Free Energy of binding to +1.1 kcal/mol. These observations suggest that the improvement in binding affinity produced by the exocyclic methyl group on dTTP is an entropic effect derived from release of dynamically restricted water during the binding reaction. Similarly, comparing the ITC data on 7Me-GTP and GTP shows that the addition of an exocyclic methyl group to this purine base increases the entropy of binding to hNBD1ΔRI by +1.2 cal/mol/°C (lower section in **Table S1**), consistent with the +2.9° increase in  $T_{SQ}$  in the presence of 7Me-GTP compared to GTP (**Figures 4B & S5B**) also being attributable to an entropy gain due to greater water released upon binding a nucleotide base with an exocyclic modification.

Another noteworthy feature in the ITC data is consistently strong entropy-enthalpy compensation when ribonucleotides vs. 2'-deoxyribonucleotides bind to hNBD1ΔRI (bottom of lower section in **Table S1**). The ribonucleotides consistently show 2-4 kcal/mol more favorable enthalpy of binding (greater heat release) and a roughly equal increase in the entropy loss upon binding, resulting in roughly equivalent binding energies for both species. The previously published hNBD1 crystal structures, as well as those reported below all, show the 2' position on the ribose ring to be fully solvent exposed, making it unlikely that the observed entropy-enthalpy compensation derives from differences in structural interactions in the bound state. Molecular dynamics calculations suggest that it derives instead from a large difference in the conformational entropy of the free nucleotides caused by the systematic differences in ribose ring pucker distribution caused by the presence or absence of the 2' hydroxyl group (unpublished results).

*X-ray crystal structures show significant variations in nucleotide-binding stereochemistry.* We determined crystal structures at ~1.9 Å resolution for F508-hNBD1ΔRI bound to 11 different nucleotide triphosphates that were characterized in

tFSQ assays (**Table S2**). Previous crystallographic studies demonstrated that the stereochemistry near the ATP-binding site in the domain is not altered by the F508del mutation (16,17). Our crystal structures show that all nucleotides bind in the canonical geometry observed for NBDs from ABC superfamily proteins (8,17,18,47) (**Figures 5 & S6**). Their triphosphate groups bind in a nearly identical geometry (**Figure S6A-B**), hydrogen bonding (H-bonding) to the lysine, threonine, serine, and final two glycine residues in the Walker A motif (GxxGxGKTS) spanning residues 458-466 and also to Gln 493 in the  $\gamma$ -phosphate switch (8,17) (alternatively called the Q-loop (48)). Their bases all adopt an *anti* configuration and make aromatic stacking interactions with the indole group of Trp 401 in the antiparallel  $\beta$  subdomain, but they adopt a wide range of positions that result in substantial differences in their closest contact to the methyl group on Thr465 in the Walker A motif (**Figures 5B-D & S6B**). This distance is 6.3 Å for the C8 atom ATP but only 4.1 Å for the exocyclic 5-methyl group in dTTP (**Figure 5B**). In structures with different nucleotides, the base effectively swings parallel to the plane of the indole group of Trp401 like a pendulum attached to a tether formed by the ribose group. The movement of the tether is produced by relatively small angular variations in the ribose group that keeps all dihedrals in the same potential energy well but collectively produce up to a 2.1 Å shift in the position of the atom on the base that is covalently bonded to the ribose group.

To gain insight into the structural basis of the thermodynamic stabilization of the domain by dTTP, we compare structures of F508-hNBD1ΔRI with dTTP vs. dUTP (**Figure 5C**), which gives a  $T_{SQ}$  3.3 °C lower than dTTP but differs exclusively by the absence of an exocyclic methyl group at the 5 position in the pyrimidine ring (**Figures 4B & S5B**). This comparison, combined with the ITC data for the binding of these two nucleotides (Table S1), suggests that the enhanced binding affinity of dTTP compared to dUTP is due to displacement of hydrating water from interaction with the methyl group on residue Thr465 in the Walker A motif. The crystal structures show a relatively subtle ~1.1 Å shift in the position of the pyrimidine rings (**Figure 5C**) in the two nucleotides, which enables the 5-methyl group on the thymine base in dTTP to make a weak 4.1 Å van der Waals contact to the methyl

group of Thr465. In contrast, the closest C5 atom in dUTP is 6.1 Å away, which leaves a gap large enough to accommodate hydrating water molecules in contact with the methyl group of Thr465. Therefore, the crystal structures suggest that the 5-methyl group in dTTP will displace water molecules interacting with the methyl group of Thr465 when dUTP is bound, which is likely to account for the +5.0 cal/mol/°C increase in the entropy of binding of dTTP compared to dUTP (Table S1). The 4.1 Å distance of the 5-methyl group on dTTP responsible for this displacement effect corresponds to an enthalpically weak van der Waals interaction. The observation that such a weak interaction can produce such significant thermal stabilization of hNBD1 suggests that a nucleotide containing a base designed to make optimal packing interactions at this site could stabilize the domain more strongly and fully offset the thermal defect caused by the F508del mutation.

Analysis of the differences in the thermodynamics of binding of GTP vs. 7Me-GTP is complicated by the fact that there is a 2.1 Å shift in the positions of their purine bases (**Figure 5D**), which is significantly larger than the shift observed for the pyrimidine bases in dTTP vs. dUTP (**Figure 5C**). Nonetheless, our structural and thermodynamic analyses suggest that the exocyclic methyl group in 7Me-GTP contributes to its increased stabilization of hNBD1 compared to GTP by dehydrating the methyl group of Thr465 in an equivalent manner to the exocyclic methyl group on dTTP. The crystal structures show that the exocyclic methyl group on 7Me-GTP is 4.0 Å away from the methyl group of Thr465, whereas the closest C8 atom on GTP is 6.7 Å away, again leaving a large enough gap to accommodate hydrating water molecules when GTP is bound but not when 7Me-GTP is bound. Our ITC data demonstrate that the latter compound has +1.2 cal/mol/°C greater entropy of binding (Table S1) and yields a +2.9 °C higher  $T_{SQ}$  (**Figure S5B**), consistent with the hypothesis that that dehydration of the methyl group of Thr465 tends to increase the entropy of binding, the affinity, and the thermal stabilization of hNBD1ΔRI by nucleotides.

Comparing structures of F508-hNBD1ΔRI with ATP vs. dATP show minimal differences in the positions or conformations of the ribose groups or

bases (**Figure S6C**). These observations support the inference presented above that the strong enthalpy-entropy compensation revealed by ITC binding assays on these compounds (Table S1) derives from differences in the conformational properties of the nucleotides in the unbound state.

*Thermal rescue of F508del-hCFTR via stabilization of hNBD1 or the NBD1-NBD2 interface.* We used temperature-controlled single-channel electrophysiology assays in black lipid membranes (6,41,49-51) to evaluate the ability of representative nucleotides to stabilize full-length F508del-hCFTR against thermal inactivation (**Figures 6 & S7**). These assays quantify not only the conductance but also the nucleotide-dependent gating kinetics (*i.e.*, opening and closing rates) of the chloride ion channel in individual functional hCFTR molecules. Channel opening is driven by formation of an hNBD1-hNBD2 interface that encapsulates two nucleotide triphosphates (13), one bound to each of these domains before interface formation, so the open probability ( $P_o$ ) of the channel at saturating nucleotide concentration provides a measure of the thermodynamic stability of the nucleotide-containing hNBD1-hNBD2 interface. The electrophysiology studies in **Figures 6 & S7** demonstrate that nucleotides that provide enhanced stabilization of either hNBD1 itself - (orange dotted lines in **Figure 1**) or the hNBD1-hNBD2 interface (green dotted lines in **Figure 1**) thermally stabilize F508del-hCFTR ion channels. These results are consistent with the thermodynamic scheme in **Figure 1**, which illustrates how compounds that bind to the native state of hCFTR (right side in **Figure 1**) stabilize it relative to the unfolded molten globule intermediate of hNBD1 (center left in **Figure 1**) that causes permanent thermal inactivation when it aggregates (top left in **Figure 1**) (10). Given this inactivation pathway, compounds with higher binding affinity that stabilize the native state more strongly should produce a greater reduction in the inactivation rate because they reduce the relative concentration of the irreversibly aggregating molten globule intermediate. The temperature-controlled electrophysiology studies in **Figures 6 & S7** verify that this mass-action mechanism produces the predicted indirect thermodynamic correction of the destabilizing effect of the F508del mutation.

At 25°C, wild-type (WT) hCFTR channels demonstrate stable gating with the same open-state conductance of  $10.6 \pm 0.1$  pS (left side of **Figure 6A**) in the presence of either ATP (green labels) or dTTP (magenta labels), which matches previously reported value measured under the same experimental conditions (41). However, the rates of channel opening and closing are both slower in the presence of 2 mM dTTP vs. ATP. The time constants for opening ( $\tau_o$ ) are 450 ms vs. 260 ms, whereas those for closing ( $\tau_c$ ) are 2.6 s vs. 750 ms, resulting in a 40% decrease in net  $P_o$  in the presence of dTTP compared to ATP ( $0.15 \pm 0.02$  vs.  $0.26 \pm 0.02$ ).

Rescued channels harboring the F508del mutation (*r*F508del-hCFTR), which are expressed in BHK cells growing at reduced temperature in the presence of the pharmacological corrector VX809, exhibit a stable open state equivalent to that adopted by WT channels but also an unstable open state with significantly lower conductance called the fast flickering mode (41) (FFM) (right side of **Figure 6A**). This pathological conductance mode has previously been observed in electrophysiological experiments on *r*F508del-hCFTR in black lipid membranes (41) but has not been reported in experiments conducted in excised membrane patches, where equivalent protein constructs show reduced channel lifetime (52-55) as well as evidence of a state with reduced conductance at physiological temperature (53). Possible reasons for the differences between experiments in black lipid membranes and excised membrane patches are outlined in the section entitled “*Temperature-dependent electrophysiology assays*” under Experimental Procedures. The FFM, which represents an early reporter of functional failure in black lipid membranes, presumably reflects a state with hNBD1 dissociated from its docking site on the TMDs due to the disruption of that interface by the F508del mutation, which leads to rapid fluctuation of the TMDs between open and closed channel conformations via a transition pathway decoupled from hNBD1-hNBD2 interface formation.

At 25 °C, *r*F508del-hCFTR alternates between the FFM and the normal gating mode in the presence of 2 mM ATP but exhibits exclusively

the normal gating mode in the presence of the same concentration of dTTP (right side of **Figure 6A**), indicating that dTTP stabilizes the physiological functional state of hCFTR more effectively than ATP. A more dramatic difference in gating properties is exhibited in experiments conducted at 30 °C in which *r*F508del-hCFTR exclusively adopts the FFM in the presence of ATP but still exclusively adopts the normal gating mode in the presence of dTTP (**Figure 6B**). Most strikingly, dTTP supported normal gating of *r*F508del-hCFTR at 37°C for ~1 minute before channel inactivation (**Figure 6C**), whereas none of the other nucleotides tested supported any channel function at this temperature. The thermodynamic studies presented above in conjunction with additional electrophysiological studies described below suggest that the qualitatively different behavior of *r*F508del-hCFTR in the presence of dTTP results from enhanced stabilization of the native conformation of F508del-hNBD1, which promotes its docking to the TMDs and formation of the proper physiological open-state conformation driven by nucleotide-mediated hNBD1-hNBD2 interaction (**Figure 1**).

We evaluated a wider range of the nucleotides characterized in our  $T_{SQ}$  assays (**Figures 4 & S5**) for their ability to support normal gating of *r*F508del-hCFTR at 30 °C. These electrophysiological assays demonstrated that a variety of deoxyribonucleotides (dATP, dGTP, dTTP, and dUTP) and the ribonucleotides TTP (5-methyl-UTP) and 7Me-GTP support at least some normal gating at this temperature, whereas the other ribonucleotides tested (ATP, GTP, and UTP) do not (**Figures 6B & S7**). To gain further insight into the thermodynamics of nucleotide interaction with hCFTR during gating, we performed full Eadie-Hofstee analyses of the gating behavior as a function of the concentration of eight representative nucleotides, four ribonucleotides (left in **Figure 6D**) and four deoxyribonucleotides (right in **Figure 6D**). We performed these analyses on WT hCFTR because *r*F508del-hCFTR is unstable and does not gate normally with some of the nucleotides at 30 °C, the temperature of our electrophysiological stabilization assays (**Figures 6B & S7**).

Eadie-Hofstee analysis of a ligand-gated

channel, which examines  $P_o$  as a function of ligand concentration, assumes channel opening depends on two factors, the effective dissociation constant or affinity of the ligand for the active conformational state of the channel undergoing gating ( $K_{eff}$ ) and the probability of adopting the open state when that ligand fully saturates its binding sites on the channel ( $P_{o-max}$ ). Given these assumptions, the observed  $P_o$  for hCFTR should show a hyperbolic dependence on nucleotide triphosphate (NTP) concentration, reflecting the dependency of gating on an equilibrium binding process:

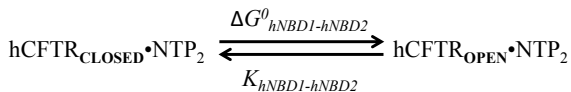
$$P_o = \frac{P_{o-max}[NTP]}{(K_{eff} + [NTP])}$$

Rearranging this equation yields a linearized form which is applied to analyzing the observed  $P_o$  as a function of varying NTP concentration:

$$P_o = P_{o-max} - K_{eff}(P_o / [NTP])$$

Therefore, the slope of the line in the resulting Eadie-Hofstee plot is the effective dissociation constant  $K_{eff}$  for a given NTP, and the intercept on the vertical axis is  $P_{o-max}$  when hCFTR is saturated by that NTP.

As indicated above, the opening of hCFTR channels is coupled to a conformational change in which spatially separated hNBD1 and hNBD2 each with a bound NTP (hCFTR<sub>CLOSED</sub>•NTP<sub>2</sub>) move together to tightly encapsulate the two bound NTPs in their mutual interface (hCFTR<sub>OPEN</sub>•NTP<sub>2</sub>) (4,5). This gating mechanism creates a simple relationship between  $P_{o-max}$  in the Eadie-Hofstee plot and the equilibrium constant ( $K_{hNBD1-hNBD2}$ ) and Gibbs Free Energy ( $\Delta G^0_{hNBD1-hNBD2}$ ) for the functional conformational change mediating hNBD1-hNBD2 interface formation and channel opening in the presence of a given NTP:



$$\begin{aligned} \Delta G^0_{hNBD1-hNBD2} &= -RT \cdot \ln(K_{hNBD1-hNBD2}) \\ &= -RT \cdot \ln(P_{o-max} / (1 - P_{o-max})) \end{aligned}$$

This formula is justified more completely and derived in the section entitled “*Relationship between the energy of hNBD1-hNBD2 interface formation and  $P_{o-max}$* ” under Experimental Procedures. The value of  $\Delta G^0_{hNBD1-hNBD2}$  should

contribute to net channel stability according the thermodynamic scheme in **Figure 1**.

The Eadie-Hofstee analyses demonstrate that the deoxyribonucleotides dATP, dGTP, and dUTP give significantly higher  $P_{o-max}$  and therefore thermodynamically stabilize the hNBD1-hNBD2 interface substantially more strongly than dTTP or the ribonucleotides ATP, GTP, UTP, and 7Me-GTP (**Figure 6D**). The 2'-hydroxyl on the ribose is completely solvent-exposed in the crystal structures of hNBD1 (**Figures 5 & S6**), making it very likely to contact hNBD2 directly in the hNBD1-hNBD2 interface in open hCFTR channels. The consistently higher  $P_{o-max}$  exhibited by the deoxyribonucleotides compared to the ribonucleotides with the same bases suggests that the 2'-hydroxyl on the ribose either loses more hydration energy or produces a mild steric clash upon packing in this interface.

Notably, the  $P_{o-max}$  values measured for the different nucleotide analogs show a different rank-order than their effective affinities  $K_{eff}$  determined in the Eadie-Hofstee analyses, which is attributable to the fact that  $K_{eff}$  depends on the binding energy of the nucleotide for both hNBD1 and hNBD2 in addition to its contribution to the stabilization energy of the functional hNBD1-hNBD2 interface, whereas  $P_{o-max}$  depends exclusively on the latter factor. The highest effective affinities are exhibited by dTTP, 7Me-GTP, and dATP. The first two nucleotides have a relatively low  $P_{o-max}$  of ~0.4-0.5 (**Figure 6D**) but provide the strongest thermal stabilization of hNBD1 (**Figure 4**), indicating that they bind most tightly to hNBD1 at its unfolding temperature. In contrast, dATP does not stabilize hNBD1 as strongly (**Figure 4**) but gives the highest observed  $P_{o-max}$  of ~0.95 (**Figure 6D**). Different nucleotides thus achieve high effective affinity via different molecular mechanisms.

To gain insight into the molecular mechanisms that enable compounds to thermally stabilize F508del-hCFTR, we plotted the value of  $\Delta G^0_{hNBD1-hNBD2}$  determined for each nucleotide against the  $T_{SQ}$  of hNBD1ΔRI measured in the presence of a 2 mM concentration of the same nucleotide, using closed symbols for the nucleotides that support normal channel gating and open symbols for those that do not (**Figure**

**6E**). This graph shows that all of the nucleotides that restore normal channel gating and thermally rescue active F508del-CFTR enhance the stability of either the hNBD1-hNBD2 interface (lower  $\Delta G^0_{\text{hNBD1-hNBD2}}$ ) or the hNBD1 domain (higher  $T_{\text{SQ}}$ ). These observations are consistent with the prediction from the thermodynamic theory that compounds that stabilize either hNBD1 directly or the hNBD1-hNBD2 interface can correct the thermodynamic defect caused by the F508del mutation in hCFTR (**Figure 1**).

### Discussion

In this paper, we use a novel thermal fluorescence self-quenching (tFSQ) assay to identify nucleotide analogs that stabilize the first nucleotide-binding domain (hNBD1) from human CFTR (hCFTR) more strongly than the physiological nucleotide ligand ATP, and we use temperature-controlled single-channel electrophysiology assays to demonstrate that these analogs also correct the thermodynamic defect in full-length hCFTR caused by the predominant disease-causing F508del mutation in hNBD1. These results represent the first conclusive demonstration of correction of this defect by a small molecule binding directly to hCFTR (31,37,53,56). Thermodynamic theory predicts that compounds with sufficient binding affinity for either the hNBD1 domain destabilized by the mutation or for the interdomain interfaces it forms in full-length hCFTR should be able to offset the thermal defect caused by the F508del mutation (**Figure 1**). Neither mode of correction has been documented convincingly in the literature to date, but our thermodynamic studies of hNBD1 (**Figures 4 & S3-S5**) combined with our electrophysiological assays on full-length hCFTR variants (**Figures 6A-D & S7**) provide examples of both modes of correction (**Figure 6E**).

Previous attempts to demonstrate direct correction of the thermodynamics defect caused by the F508del mutation focused on identification of small molecules that bind to hNBD1. Several compounds with relatively weak micromolar-level affinity for hNBD1 have been identified (39,57), but none of these compounds have been demonstrated to thermally rescue full-length F508del-CFTR. One such compound called RDR1 was identified using differential scanning

fluorimetry (DSF) assays that monitor the unfolding of hNBD1 indirectly based on interaction of the unfolded conformation of the protein with a fluorescent reporter dye (40,58). Our tFSQ assays failed to reproduce the stabilizing effect on hNBD1 inferred from DSF assays (**Figure S8**), and DSC assays also fail to show any improvement in the thermal stability of hNBD1 in the presence of this compound (59). In contrast, our electrophysiological assays (**Figure 6**) demonstrate that nucleotides that stabilize hNBD1 (dTTP and 7Me-GTP in **Figure 4**) and different nucleotides that stabilize the functional hNBD1-hNBD2 interface (dATP, dGTP, and dUTP in **Figure 6D-E**) both restore normal channel gating and rescue the thermal defect in F508del-hCFTR.

A wide variety of “corrector” compounds improving F508del-hCFTR biogenesis *in vivo* have been identified using cell-based assays (60-62), but their mechanisms-of-action (31,37,53,56) and binding sites remain unclear, which has prevented use of structure-based methods to improve their efficacy. The uncertainty concerning mechanism-of-action has left lingering doubt whether they bind directly to hCFTR or have a different molecular target. Importantly, none of these compounds have been demonstrated to thermally stabilize hCFTR molecules on a physiologically relevant timescale (31,37,53,56). The corrector compound, VX809 or Lumacaftor, which has been approved for clinical use in humans, produces functional expression of F508del-hCFTR at ~14% of that of WT hCFTR (60). There are conflicting reports in the literature concerning whether Lumacaftor provides effective short-term stabilization of CFTR channel function *in vivo* on the timescale of minutes (31,37,53,63), and one recent paper demonstrated significant thermodynamic destabilization of isolated hNBD1 in DSC experiments conducted in the presence of 1 mM Lumacaftor (63). Although additional research will be required to resolve this controversy, it is clear that Lumacaftor does not fully correct the thermal stability defect caused by the F508del mutation in full-length CFTR (31), and it does not support any proper channel gating at 37 °C in the temperature-dependent electrophysiology assays employed in this paper (31), while dTTP does (**Figure 6C**). The thermally destabilizing influence of the F508del mutation promotes more rapid degradation at 37 °C, which reduces the steady-state

level of F508del-CFTR in the plasma membrane. The results reported in this paper prove that thermal stabilization of hCFTR channel function (**Figures 6 & S7**) can be achieved by a compound binding directly to hCFTR (**Figures 5 & S6**).

The previously identified corrector compounds improve functional expression of hCFTR, but their inability to correct the thermal stability defect suggests that they may modulate its biogenesis pathway rather than binding directly to the protein. These compounds were all identified using cell-based screens, so their molecular target is not necessarily hCFTR. Most corrector compounds were identified using assays measuring F508del-hCFTR ion conductance in the plasma membrane of living cells (60-62), and their molecular targets have not been conclusively established. In contrast, the molecular target is known for a corrector recently identified using an alternative cell-based screen for compounds that increase the level of immature F508del-hCFTR (band B) in the endoplasmic reticulum (ER) without changing its mRNA level. One compound identified using this screen, PYR-41, is a known inhibitor of an E1 ubiquitin-activating enzyme, and it increases the level of functional, mature protein (band C) in the plasma membrane by reducing the rate of proteolytic degradation of F508del-hCFTR (62). This compound provides a clear example of a corrector that modulates hCFTR biogenesis indirectly rather than by binding directly to CFTR. Correctors that do not bind directly are unlikely to thermally stabilize F508del-hCFTR, in which case they cannot correct one of the two molecular defects caused by the F508del mutation. In contrast, the nucleotide analogs analyzed in this paper bind directly to hCFTR, and, as predicted by thermodynamic theory, they correct the fundamental thermodynamic defect caused by the F508del mutation and thermally stabilize F508del-CFTR molecules.

Our calorimetric (**Figures 4C-E & Table S1**) and crystallographic (**Figures 5 & S6**) studies suggest that a nucleotide with a custom base designed using computational chemistry methods could fully rescue the thermal defect caused by the F508del mutation. This observation is noteworthy, because a variety of nucleotide analogs are clinically approved and effective drugs (64-66). We

observe that two nucleotides with sub-optimal packing interactions (**Figure 5**), dTTP and 7Me-GTP, stabilize hNBD1ΔRI more strongly than the major physiological ligand ATP and offset approximately half of the 6.8 °C reduction in its thermal unfolding temperature produced by the F508del mutation (**Figure 2C**). The exocyclic methyl groups on the bases of these nucleotides are likely to displace entropically restricted water molecules hydrating the hydrophobic methyl group on the sidechain of residue Thr465 in Walker A motif (GxxGxGKTS) spanning residues 458-466 in hCFTR, thereby producing an entropy increase upon binding due to the reduction in solvent-exposed hydrophobic surface area (**Figures 4C-E & Table S1**). However, the internuclear distances between the methyl group of Thr465 and the exocyclic methyl groups on dTTP and 7Me-GTP are 4.1 and 4.0 Å, respectively, which represents a sub-optimal and energetically weak van der Waals contact. A nucleotide with a base making optimal packing interactions in this binding site would have the same entropic advantage while also having larger interaction enthalpy, which would increase binding affinity for hNBD1 and enhance its thermal stabilization.

The observation that a 0.5 kcal/mol difference in the binding affinity of dTTP compared to ATP (**Figure 4E and Table S1**) offsets half of the thermal defect caused by the F508del mutation (**Figures 2C, 4A-D, & S3B**) suggests that a relatively small gain in nucleotide-binding affinity should completely offset the thermal defect at the therapeutic concentration for most drugs, which is typically in the low micromolar range. Physiologically, dTTP is present at a similar concentration of ~30 μM (67), which is approximately 1/100 of the cellular concentration of ATP. Given the comparative binding affinities and cellular concentrations of dTTP vs. ATP, the former only provides ~1/30 of the stabilization of the latter under physiological conditions. We estimate that an increase in binding energy compared to dTTP on the order of ~3 kcal/mol, which corresponds to an ~160-fold increase in equilibrium constant, would be needed for a appropriately designed nucleotide analog to fully offset the thermodynamic defect caused by the F508del mutation at the low micromolar concentrations typically achieved for the related

drugs currently in clinical use (64). Nucleotide analogs are widely used in human pharmacology thanks to the presence of promiscuous kinases in human cells that phosphorylate the corresponding nucleosides, which are generally cell-permeable (68,69). Notably, the dTTP analogs azidothymidine triphosphate and d4TTP (65), the triphosphate derivatives of Zidovudine (66) and Stavudine (66), remain among the most widely used antiviral drugs worldwide (70).

The technical characteristics of our fluorescence self-quenching (FSQ) assay (**Figure 3**) demonstrate that equivalent assays should be a powerful tool for high-throughput screening to identify small molecule lead compounds to treat the many human protein-folding diseases that involve aggregation. Our results demonstrate that FSQ is equivalently effective in monitoring protein aggregation when implemented in thermal-ramping assays (tFSQ – **Figures 4 & S3-5**) or isothermal kinetic assays (iFSQ – **Figure S2**). The excellent sensitivity of the assay derives from the high signal-to-noise ratio provided by fluorescence detection combined with the nonlinear dependence of self-quenching on aggregate size. Monitoring protein stability in this indirect manner based on subsequent aggregation provides a very large gain in sensitivity compared to the available biophysical methods that monitor unfolding directly. Furthermore, our data demonstrate that using FSQ to monitor unfolding/aggregation provides exceptional precision and reproducibility (**Figures 3B-C, 4A-B, & S3-5**) while closely tracking the results obtained from rigorous thermodynamic assays (**Figures 4C-E**) that require large amounts of protein and that are too slow and cumbersome to be used for high-throughput screening. Many protein unfolding reactions induce aggregation (71,72), and a wide variety of serious and prevalent human diseases are caused by toxic protein aggregation processes (73-75), some of which are triggered by destabilizing mutations, as is the case for F508del mutation in hCFTR (1). The results reported in this paper on hNBD1 and hCFTR demonstrate that the FSQ assay provides excellent performance screening for compounds that prevent protein aggregation. Therefore, tFSQ and iFSQ assays equivalent to those implemented in this paper should be applicable to screening for correctors to treat diseases caused by protein

aggregation (73-75) as well as diseases caused by protein destabilization when unfolding of the protein triggers aggregation (71,72). Moreover, the thermodynamic stabilization strategy (**Figure 1**) proven to work in our studies of nucleotide interaction with F508del-hCFTR (**Figures 6 & S7**) should be applicable to treating diseases caused by protein instability.

### Experimental Procedures

*Computational prediction of protein stability changes induced by Cys-reduced mutations.* Starting from the crystal structure of F508-hNBD1 $\Delta$ RI (PDB id 2PZE), we reconstructed missing sidechains using the Eris protein design suite (76). We repaired breaks in the protein backbone using discrete molecular dynamics (DMD) (77-79) with peptide bond distance and angular constraints connecting the broken fragments. We allowed three residues on each side of the break to move freely to fulfill the constraints, while the rest of the protein remained static. We performed mutations to the structure and calculated the  $\Delta\Delta G$  using the Eris suite (45,80). We ensured that the residues binding ATP did not move significantly in any step of the procedure. The prediction of protein stability changes by mutations is also available online via the Eris server (45,80).

*Protein engineering and purification of thermally stable hNBD1 constructs.* Based on a QuikChange protocol of site-directed mutagenesis (Agilent Technologies, CA, USA), the Cys-reduced constructs were engineered from truncated F508- and F508del- hNBD1 domains that were used in previously published studies. In brief, the constructs comprise residues 387–646 of human CFTR with residues 405–436 deleted. All the Cys-reduced hNBD1 constructs were expressed in *E. coli* at 18°C and purified using previously published methods. The domains with an N-terminal His<sub>6</sub>-Smt<sub>3</sub> fusion were purified by Ni-NTA chromatography, cleaved by Ulp1 protease, purified by Sephacryl S200 gel filtration chromatography, recovered from the flow-through of a second Ni-NTA column (to remove residual His<sub>6</sub>-Smt<sub>3</sub> tag), and concentrated to 2–5 mg in Standard Stabilizing Buffer.

*Visible fluorescence covalently labeling on Cys-reduced hNBD1 domains.* 1 mg of AlexaFluor 546

(AF546) C<sub>5</sub> maleimide power was first dissolved in 200  $\mu$ L of fresh anhydrous dimethyl sulfoxide (D8418, Sigma-Aldrich, USA) right before hNBD1 labeling. A tenfold higher amount of the fluorescence dye was mixed with the protein at  $\sim$ 20  $\mu$ M concentration (0.5 mg/mL) in the Standard Stabilizing Buffer. The labeling mixture was incubated at room temperature for 5 minutes and was then chilled on ice for another 5 minutes. Then a 1000-fold higher amount of 2-mercaptoethanol, compared with the AF546 dye, was added to the mixture to terminate the labeling reaction. An excess amount of free fluorescence dye in the mixture was first roughly removed by a PD-10 desalting column and was then further separated by gel filtration chromatography in the Standard Stabilizing Buffer. Purified AF546-labeled proteins were eventually concentrated up to around 120  $\mu$ M (3 mg/mL) with a degree of labeling around 0.9.

*Thermal fluorescence self-quenching assays.* Thermal fluorescence self-quenching assay in circular dichroism (CD) setup was conducted with a J-815 spectropolarimeter (with a 1.6 mL cuvette volume) (Jasco, Easton, USA) equipped with a PFD-425 Peltier temperature-controlled cell, an FMO-427 fluorescence detector. Control temperature was monitored in the CD cuvette by its operating computer and heating rate was 3  $^{\circ}$ C per minute. Thermal self-quenching assay in real-time PCR plate format (96-well or 384-well, 10  $\mu$ L solution volume) was conducted in Mx3500P qPCR system (Agilent Technologies, USA) for 96-well PCR plate and in ViiA 7 real-time PCR system (Life Technologies, USA) for 384-well PCR plate. Heating rate in qPCR setups was consistently conducted at 3  $^{\circ}$ C per minute. Fluorescence monitoring wavelengths were excitation at 545 nm and emission at 568 nm. Data processing and T<sub>SQ</sub> temperature determination were conducted using GraphPad Prism 5 software (GraphPad Software, Inc., USA). AF546 labeled protein was firstly diluted from the protein stock down to 0.005 mg/mL ( $\sim$ 0.2  $\mu$ M) as protein working solution in tFSQ assays. 100 mM of eight native nucleotides or nucleotide analogs were added to each well with a volume ratio between protein working sample and nucleotide at 50:1 to reach final desired nucleotide concentrations. Similar to nucleotide tFSQ evaluation, the RDR1 compound was firstly dissolved in DMSO at 80 mM to prepare viable

stock concentrations which were 50-fold higher than final working RDR1 concentrations in the tFSQ assay.

*Differential scanning calorimetry (DSC).* Calorimetry was carried out with a VP-Capillary DSC System (MicroCal Inc., GE HealthCare, Piscataway, NJ) in 0.130 mL cells at 2  $^{\circ}$ C per min. An external pressure of 2.0 atm was maintained during all DSC runs to prevent possible degassing of the solutions upon heating. The DSCs were conducted in the Standard Stabilizing Buffer. ATP-free protein stock solution was prepared as the following: the ATP was removed by repeatedly diluting the sample 10-fold into the Mg-ATP free buffer and then concentrating back to the original volume using an Amicon ultrafiltration device with an MWCO of 10 kDa. A total of 5 diluting/concentrating cycles were performed. 2 mM EDTA was included in the buffer for the first 3 cycles to ensure residual magnesium removal. Before thermal unfolding, various amounts of the nucleotides or analogs were added to the protein sample and incubated at 5  $^{\circ}$ C for at least 1 hour.

Protein concentration was determined using the Pierce BCA kit in a microtiter plate. *Bacillus subtilis* NAD synthetase was used to establish the protein concentration calibration curve each time this assay was performed. The standard deviation among triplicate samples was usually less than 5%. The protein concentration assay was also validated to ensure accuracy using an hNBD1 sample with known concentration that was determined by quantitative amino acid analysis. DSC was conducted at a protein concentration of 20  $\mu$ M. DSC data were analyzed with the Origin 7.0 software (OriginLab, Northampton, MA), from which the unfolding temperature (T<sub>m</sub>), and the calorimetric unfolding enthalpy ( $\Delta$ H<sub>c</sub>) were obtained.

*Isothermal Titration Calorimetry (ITC).* F508-hNBD1 $\Delta$ RI was purified as previously described (10,11) and stored in Standard Stabilizing buffer. Immediately before the titration experiments, ATP was removed as described in for DSC experiments. The residual ATP concentration in the protein was determined by an HPLC assay, as previously described (81). Briefly, 100  $\mu$ L of the protein sample were mixed with 100  $\mu$ L of 6 M guanidine-

HCl to completely denature the protein and release any bound ATP, and 30  $\mu\text{L}$  of the denatured protein sample was analyzed on a  $4.6 \times 100$  mm Synergi Polar-RP column (Phenomenex, Torrance, CA) connected to a Shimadzu (Durham, NC) HPLC system. The ATP concentration calibration curve was established using pure ATP in the same buffer. The detection limit of this method was 0.025  $\mu\text{M}$  ATP. Measured ATP concentrations after ATP removal did not exceed 1  $\mu\text{M}$  and in most cases were less than 0.5  $\mu\text{M}$ . The nucleotide solutions were prepared by diluting a 100 mM stock into the matching buffer, which was the filtrate from the ultrafiltration device during the last step of protein concentration. The nucleotide concentration was verified by UV absorbance using the extinction coefficients provided by the manufacturer (Thermo-Fisher, Waltham, MA). 3 mM  $\text{MgCl}_2$  was added to both the protein and the nucleotide solutions before the titration experiments.

ITC experiments were performed using a MicroCal Auto-iTC200 System (Malvern Instruments, Malvern, UK). In each experiment, 0.2 mM nucleotide was transferred to the injection syringe, and 20 – 25  $\mu\text{M}$  hNBD1 was transferred into the cell by the autosampler. Before being transferred, the samples were stored in a 96-well sample plate inside the sample holder, which was maintained at 5  $^\circ\text{C}$ . The titrations were carried out at 10  $^\circ\text{C}$ . Each titration experiment consisted of 10 injections of 2  $\mu\text{L}$  each, followed by 6 injections of 3  $\mu\text{L}$  each. The interval between injections was 300 seconds. The instrument feedback gain was set to 'none' to reduce noise. Data analysis was performed using the MicroCal Origin 7.0 (OriginLab Corp., Northampton, MA) curve-fitting routines supplied with the instrument. The binding parameters, which included the stoichiometry ( $N$ ), the binding constant ( $K$ ) and the binding enthalpy change ( $\Delta H$ ), were determined by fitting the integrated heats using the Origin curve-fitting for one set of identical binding sites. The software calculated the entropy change ( $\Delta S$ ) for the binding, and the Gibbs free energy change ( $\Delta G$ ) was calculated as  $\Delta G = -RT \cdot \ln(K)$ , where  $R$  is the ideal gas constant and  $T$  is the absolute temperature (283.15  $^\circ\text{K}$ ).

We investigated possible causes for the low (< 1:1) values of binding stoichiometry consistently obtained from our ITC data on hNBD1. We

concluded this phenomenon is attributable to a portion of the protein population forming aggregates during the ITC experiments that are incapable of binding nucleotides, and we performed analyses demonstrating that the thermodynamic binding parameters determined under such circumstances should remain accurate. Protein aggregation under the conditions of our ITC experiments is consistent with the observation of some precipitate in the sample recovered from the cell after every titration and furthermore with the known biophysical properties of hNBD1. As summarized in the main text and described in detail in previous papers (10,11,17), ATP binding strongly destabilizes the domain compared to a rapidly aggregating molten-globule conformation with minimal affinity for ATP. Due to this effect, the domain is purified in the presence of ATP, which has to be removed in order to perform an ITC experiment, and removal of ATP from the protein solution is expected to accelerate formation of protein aggregates that are incapable of binding ATP. We ruled out alternative explanations related to errors in concentration determination or carry-over of residual ATP from the buffer used to purify the protein. Nucleotide concentrations were determined based on UV absorbance and closely matched expected values based on calculations. Protein concentration before the ITC experiments was verified using the Pierce 660 nm Protein Assay Reagent (ThermoFisher Scientific), and the purity of the protein as assessed by SDS-PAGE was >95%. Finally, the HPLC method described above demonstrated that the amount of ATP carryover was always less than 5% of the total protein concentration.

Importantly, loss of active protein due to aggregation during an ITC experiment is not expected to change the measured value of the binding enthalpy as long as the experiment is conducted in the proper regime in which the concentration of active protein molecules greatly exceeds the dissociation constant for the binding reaction, which was the case in all of our ITC experiments on hNBD1 (*i.e.*, active protein concentrations > 8  $\mu\text{M}$  compared to dissociation constants < 0.9  $\mu\text{M}$ ). In this regime, nearly all incoming ligand molecules bind to protein molecules at the early points in the titration, and the enthalpy of binding is given directly by the

measured value of kcal of heat per mole of injectant in this region. Thermodynamic parameters can only be inferred reliably from curve fitting of ITC experiments conducted in this regime in which the measured value of enthalpy is essentially independent of active protein concentration (82). To confirm the insensitivity of the thermodynamic parameters inferred from our ITC experiments to variations in active protein concentration, we performed curve fitting of our data assuming that 50% of the protein population was inaccessible for nucleotide binding, and we obtained ~1:1 binding stoichiometry without significant changes in the values of the binding enthalpy or entropy or the dissociation constant (unpublished data).

*Crystallization and structure determination of truncated F508-hNBD1 with dTTP and dTTP analogs.* F508-hNBD1 $\Delta$ RI for crystallization was purified using a modified protocol as described before (10,11). However, the dialyzed buffer during the Ni-NTA purification was changed to an ATP-free buffer containing 150 mM NaCl, 30% (v/v) glycerol, 1 mM TCEP, and 20 mM Na-HEPES pH 7.5 to remove imidazole and ATP from the protein. In size-exclusive gel-filtration purification, the buffer was then switched back to SSB without any nucleotide. Then the purified protein was concentrated up to 10 mg/mL using Amicon Ultra-15 centrifugal filters with MWCO of 10 kDa. 2mM of dTTP or ATP was added into protein buffer before concentration. Co-crystallization of the concentrated protein with the nucleotides was conducted in microbatch 72-well plates using vapor diffusion method under 100% paraffin oil with an incubation temperature at 6 °C. Precipitant buffer contains 40% (v/v) PEG 400, 100 mM NH<sub>4</sub>Cl, and 100 mM MES pH 6. The volume ratio of the protein and precipitant was set at 1:3. After 5-7 days' incubation and equilibration at 4 °C, each drop was streak seeded using a human hair. Protein crystals over 100  $\mu$ m were mounted into CrystalCap HT<sup>TM</sup> (SPINE) with 15% glycerol as cryoprotectant. The mounted crystals were then stored in liquid nitrogen after liquid nitrogen snap-freezing. 7Me-GTP-bound protein crystals were obtained by ligand soaking (83) from dTTP-bound crystals. Other nucleotide-bound (dATP, dGTP, dCTP, dUTP, GTP, CTP, UTP, TTP (5-methyl-UTP)) protein crystals were soaked from ATP-bound crystals. In brief, dTTP-bound/ATP-bound hNBD1 $\Delta$ RI crystals were

first transferred into a cryoprotectant containing 4 mM Mg-nucleotides in a clean micro batch 72-well plate covered with 100% paraffin oil. After 24 hours of incubation at 4 °C, the soaked crystals were transferred into separate identical fresh cryoprotectant wells with the same appropriate nucleotides at 4 °C for additional 7 days. A second one-week incubation at 4 °C was conducted with fresh nucleotides before the nucleotide-bound hNBD1 $\Delta$ RI crystals were mounted and stored in liquid Nitrogen. X-ray diffraction data were collected using X4C synchrotron beamline at the National Synchrotron Light Source at Brookhaven National Laboratory or BL14-1 Stanford Synchrotron Radiation Lightsource. Diffraction data were indexed and integrated using HKL (84) software. Structure modeling, building, refinement, and evaluation were conducted using molecular replacement method from PHENIX software (85). The published hNBD1 structure (PDB id 2PZE) was used as the molecular replacement model.

*Membrane isolation for electrophysiology.* Membrane vesicles containing thermally stable wild-type hCFTR were prepared from BHK cells stably expressing wild-type hCFTR as described previously (41). Some modifications were introduced for membrane vesicle preparation to allow BHK cells to stably express F508del-CFTR. Corrector plus low temperature-rescued human rF508del-hCFTR (31) was used. BHK cells stably expressing F508del-hCFTR were grown under standard conditions in a 150 mm dish up to 80% confluence before shifting to reduced temperature (28 °C) for 48 hours during which the small molecule corrector VX809 was present in the last 12 hours. After treatment, cells were harvested by scraping, pelleted by brief centrifugation, and resuspended in ice-cold hypotonic lysis buffer containing 5 mM ATP. Following a 15-min-incubation on ice, cells were lysed by 10 strokes in a tight-fitting Dounce homogenizer, followed by an additional 15 strokes after the addition of an equal volume of sucrose buffer was centrifuged at 100,000g for 45 min to sediment microsomes which were then resuspended in phosphorylation buffer. The expression of the mature form of the rF508del-hCFTR protein was confirmed by immunoblotting. Membrane vesicles were phosphorylated by incubation with 50 nM PKA catalytic subunit in phosphorylation buffer containing 5 mM ATP for

15 min at room temperature. The membranes containing rescued F508del-hCFTR were always stored on ice and used for the functional assay the same day.

*Planar-bilayer based single-channel electrophysiology.* Planar lipid bilayers were prepared by painting a 0.2-mm hole drilled in a Teflon cup with a phospholipid solution in *n*-decane containing a 3:1 mixture of 1-palmitoyl-2-oleoyl-snglycero-3-phosphoethanolamine and 1-palmitoyl-2-oleoyl-snglycero-3-phosphoserine. The lipid bilayer separated 1.0 mL of solution in the Teflon cup (*cis* side) from 5.0 ml of a solution in an outer glass chamber (*trans* side). Both chambers were magnetically stirred and thermally insulated. Heating and temperature control were established by the temperature control system TC2BIP (Cell Micro Controls, USA). CFTR ion channels were transferred into the preformed lipid bilayer by spontaneous fusion of membrane vesicles containing the wild-type hCFTR (WT-hCFTR) or VX809 and temperature rescued F508del hCFTR (*r*F508del-hCFTR) in symmetrical salt solution. Single-channel currents were recorded at -75 mV under voltage-clamp conditions using an Axopatch 200B amplifier (Molecular Devices, LLC., Sunnyvale, CA). For analysis, the single-channel current was digitized by Digidata 1322 (Molecular Devices, LLC., Sunnyvale, CA) with a sampling rate of 500 Hz and analyzed using pCLAMP 9.2 software (Molecular Devices, LLC. Sunnyvale, CA). Origin 7.5 (OriginLab Corp., Northampton, MA) was used to fit all-point histograms by multi-peak Gaussians. Single-channel current was defined as the distance between peaks on the fitting curve and was used for the calculation of the single-channel conductance. The single-channel open probability ( $P_o$ ) was calculated as the ratio of the area under the peak for the open state to the total area under both peaks on the fitting curve.

*Temperature-dependent electrophysiology assays.* Heating and temperature control were established by the temperature control system TC2BIP (Cell Micro Controls, Norfolk, VA, USA). The values of the temperatures in the bulk solution and in the vicinity of the single channel were confirmed when the open-state conductance was identical to that of the wild-type hCFTR at the same bulk solution temperature (41) at thermal equilibrium. Possible

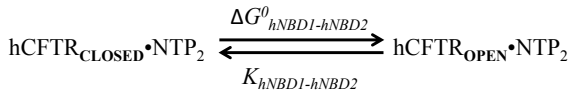
differences in the gating kinetics of the WT vs. F508del-hCFTR constructs were not taken into account.

Thermal stability of an hCFTR construct was defined based on its ability to demonstrate single channel function with open state conductance identical to the wild-type hCFTR under the same experimental conditions for a 10-min period following an initial 10 min of incubation at the indicated temperature. Consistent with this definition, each recording in **Figure 6B** shows the last 2 min of a 20 min recording at 30 °C, demonstrating a dramatic difference in the thermal stability of *r*F508del-hCFTR in the presence of a 2 mM concentration of different nucleotide analogs.

As previously reported, *r*F508del-hCFTR produced in BHK cells using the protocol employed here exhibits several gating modes in black lipid membranes including including a fast-flickering mode (FFM) with an unstable and less conductive open state (41). The FFM is a hallmark of CFTR thermal instability that becomes apparent at the elevated temperature of 30 °C, and it was interpreted to represent an initial step in the functional inactivation of *r*F508del-hCFTR in black lipid membranes (41). The FFM has not been reported in experiments conducted on similar F508del-hCFTR protein constructs in excised membrane patches, although these experiments confirm that the mutation reduces functional protein lifetime (52-55) and some show evidence of an open-channel state with reduced conductance (53). The failure to observe the FFM in studies on excised membrane patches could be attributable to differences in protein preparation procedures, differences in the lipid composition in the membranes used for the electrophysiological measurements, or differences in the observation protocol. Our *r*F508del-hCFTR preparations typically shown normal open-state conductance at the beginning of experiments conducted at room temperature prior to the appearance of the FFM later during the 20-min time period over which measurements are conducted.

*Relationship between the energy of hNBD1-hNBD2 interface formation and  $P_{o-max}$ .* Previous research has demonstrated that hNBD1 is catalytically inactive (17,18,86,87). Therefore, assuming

diphosphate/triphosphate exchange occurs rapidly compared to NTP binding and hydrolysis by hNBD2, both hNBD1 and hNBD2 will have NTPs bound the vast majority of the time in the presence of a saturating NTP concentration, which is the condition that yields  $P_{o-max}$  in the Eadie-Hofstee analysis. Because channel opening and closing rates have both been shown to be independent of NTP concentration under saturating conditions (88-90), the dynamics of channel gating at saturation are well approximated as a simple two-state equilibrium in which individual hCFTR channels cycle between an open conformation with two triphosphates encapsulated in the hNBD1-hNBD2 interface (hCFTR<sub>OPEN</sub>•NTP<sub>2</sub>) and a closed conformation in which hNBD1 and hNBD2 are spatially separated but still both have bound NTPs (hCFTR<sub>CLOSED</sub>•NTP<sub>2</sub>):



This gating model assumes that, at a saturating concentration of a given NTP, all hCFTR molecules have that NTP species bound to both hNBD1 and hNBD2 the vast majority of the time and that the observed differences in the open probability ( $P_{o-max}$ ) reflect different proportions of channels occupying the open (hCFTR<sub>OPEN</sub>•NTP<sub>2</sub>) vs. closed (hCFTR<sub>CLOSED</sub>•NTP<sub>2</sub>) conformational states when that NTP is bound. The different proportions in the two states reflect variations in the equilibrium constants ( $K_{\text{hNBD1-hNBD2}}$ ) and corresponding Gibbs Free Energy changes ( $\Delta G^0_{\text{hNBD1-hNBD2}}$ ) for the conformational transition when the different NTPs are bound to the protein:

$$\begin{aligned} (1/\tau_c)[\text{hCFTR}_{\text{OPEN}} \cdot \text{NTP}_2] &= (1/\tau_o)[\text{hCFTR}_{\text{CLOSED}} \cdot \text{NTP}_2] \\ [\text{hCFTR}_{\text{OPEN}} \cdot \text{NTP}_2] / [\text{hCFTR}_{\text{CLOSED}} \cdot \text{NTP}_2] &= (\tau_c / \tau_o) \\ &= K_{\text{hNBD1-hNBD2}} \\ &= P_{o-max} / (1 - P_{o-max}) \\ \Delta G^0_{\text{hNBD1-hNBD2}} &= -RT \cdot \ln(K_{\text{hNBD1-hNBD2}}) \\ &= -RT \cdot \ln(P_{o-max} / (1 - P_{o-max})) \end{aligned}$$

The parameters  $\tau_o$  and  $\tau_c$  in the equations above are the time constants for channel opening and closing, respectively. The population ratio ( $P_{o-max} / (1 - P_{o-max})$ ) from single-channel recordings corresponds to  $K_{\text{hNBD1-hNBD2}}$  because, according to basic statistical

mechanical principles, the fraction of time an individual channel spends in the open vs. closed conformation will match the steady-state distribution of open vs. closed channels in a population of hCFTR molecules at equilibrium. While the individual time constants  $\tau_o$  and  $\tau_c$  depend on the activation energy for channel opening, which should not influence net channel stability,  $\Delta G^0_{\text{hNBD1-hNBD2}}$  depends on their ratio, which is independent of activation energy and contributes directly to net channel stability according to the thermodynamic scheme in **Figure 1**.

The assumption underlying this model concerning rapid diphosphate/triphosphate exchange on hNBD2 following hydrolysis must be correct for dATP and dGTP, the two NTPs giving  $P_{o-max}$  values close to 1.0 (**Figure 6D**), because opening of the hCFTR channel requires an NTP to be bound to hNBD2 (4,5). Therefore, an open probability close to 1 can only be achieved if hNBD2 has an NTP bound in its active site close to 100% of the time, which requires rapid replacement of the diphosphate product by the triphosphate substrate following each round of hydrolysis. Our assumption that the other six NTPs characterized in **Figure 6** undergo comparably rapid diphosphate/triphosphate exchange on hNBD2 even though they give lower  $P_{o-max}$  values seems reasonable based on several considerations. These NTPs have Gibbs Free Energies of binding to isolated hNBD1 that differ by only  $-1.0$  to  $+0.5 \pm 0.2$  kcal/mole at  $10^\circ\text{C}$  compared to dATP (**Table S1**), making it unlikely they have dramatic differences in affinity for hNBD2 given the strong homology of its nucleotide-binding site to that in hNBD1. More importantly, the NTPs showing lower values of  $P_{o-max}$  have effective binding affinities for the open state of the hCFTR channel, as given by the slopes in the Eadie-Hofstee plots in **Figure 6D**, that vary from 2.2-fold higher to 16-fold lower than that of dATP, the species giving the highest  $P_{o-max}$ . The observation that none of the NTPs has more than very slightly higher effective affinity for hCFTR than the rapidly exchanging nucleotide dATP makes it unlikely they undergo much slower diphosphate/triphosphate exchange on hNBD2 than dATP. These observations provide support for our assumption that all of the NTPs characterized in **Figure 6** undergo rapid diphosphate/triphosphate exchange on hNBD2 following hydrolysis.

### **Acknowledgements**

The authors thank Cystic Fibrosis Foundation Therapeutics Inc. for long-term support of research by the CFTR 3D Structure Consortium, including the work reported in this paper. We thank Patrick Thibodeau and the other members of the CFTR 3D Structure Consortium for advice. FF was supported by grant 5U54GM094597 from the Protein Structure Initiative of the NIH to the Northeast Structural Genomics Consortium. NVD acknowledges support by NIH grants R01GM114015 and R01GM123247. The laboratory group of BRS was supported by NIH grant 1R35CA209896, and AK was supported by grant T32GM008281 from the NIH Training Program in Molecular Biophysics.

### **Conflict of interest**

The authors declare that they have no conflict of interest.

### **Author contributions**

JFH and CW conceived the project. They designed the thermodynamic experiments with ZY, CGB, AK, and BRS and the electrophysiological experiments with AAA and JRR. Molecular mechanics calculations for protein engineering were de-signed and performed by EAP, PK, and NDD. Molecular dynamics simulations to interpret thermodynamic data were designed and performed by NK and HS. CW, FF, and JA performed the protein-engineering and crystallographic experiments. CW, ZY, JA, and AK performed the thermodynamic experiments. AAA performed the electrophysiological experiments. JFH and CW drafted and finalized the manuscript with contributions from all authors.

### **§ Current address**

Farhad Forouhar is in Irving Cancer Research Center, Columbia University, New York, NY 10032, USA; Elizabeth A. Proctor is in Department of Biological Engineering, Massachusetts Institute of Technology, Cambridge, MA 02139, USA; Pradeep Kota is in NCI-Frederick, Laboratory of Cell and Developmental Signaling, MD 21702, USA; Grégory Boël is in the Institut de Biologie Physico-chimique, CNRS UMR8261, Université Paris Diderot, Sorbonne Paris Cité, 13 rue Pierre et Marie Curie, Paris, France.

## References

1. Riordan, J. R., Rommens, J. M., Kerem, B., Alon, N., Rozmahel, R., Grzelczak, Z., Zielenski, J., Lok, S., Plavsic, N., Chou, J. L., and et al. (1989) Identification of the cystic fibrosis gene: cloning and characterization of complementary DNA. *Science* **245**, 1066-1073
2. Frizzell, R. A., and Hanrahan, J. W. (2012) Physiology of epithelial chloride and fluid secretion. *Cold Spring Harb Perspect Med* **2**, a009563
3. Cutting, G. R., Kasch, L. M., Rosenstein, B. J., Zielenski, J., Tsui, L. C., Antonarakis, S. E., and Kazazian, H. H., Jr. (1990) A cluster of cystic fibrosis mutations in the first nucleotide-binding fold of the cystic fibrosis conductance regulator protein. *Nature* **346**, 366-369
4. Vergani, P., Lockless, S. W., Nairn, A. C., and Gadsby, D. C. (2005) CFTR channel opening by ATP-driven tight dimerization of its nucleotide-binding domains. *Nature* **433**, 876-880
5. Mense, M., Vergani, P., White, D. M., Altberg, G., Nairn, A. C., and Gadsby, D. C. (2006) In vivo phosphorylation of CFTR promotes formation of a nucleotide-binding domain heterodimer. *The EMBO journal* **25**, 4728-4739
6. Yoo, J. S., Moyer, B. D., Bannykh, S., Yoo, H. M., Riordan, J. R., and Balch, W. E. (2002) Non-conventional trafficking of the cystic fibrosis transmembrane conductance regulator through the early secretory pathway. *J Biol Chem* **277**, 11401-11409
7. Riordan, J. R. (2005) Assembly of functional CFTR chloride channels. *Annu Rev Physiol* **67**, 701-718
8. Smith, P. C., Karpowich, N., Millen, L., Moody, J. E., Rosen, J., Thomas, P. J., and Hunt, J. F. (2002) ATP binding to the motor domain from an ABC transporter drives formation of a nucleotide sandwich dimer. *Mol Cell* **10**, 139-149
9. Hunt, J. F., Wang, C., and Ford, R. C. (2013) Cystic fibrosis transmembrane conductance regulator (ABCC7) structure. *Cold Spring Harb Perspect Med* **3**, a009514
10. Protasevich, I., Yang, Z., Wang, C., Atwell, S., Zhao, X., Emtage, S., Wetmore, D., Hunt, J. F., and Brouillette, C. G. (2010) Thermal unfolding studies show the disease causing F508del mutation in CFTR thermodynamically destabilizes nucleotide-binding domain 1. *Protein Sci* **19**, 1917-1931
11. Wang, C., Protasevich, I., Yang, Z., Seehausen, D., Skalak, T., Zhao, X., Atwell, S., Spencer Emtage, J., Wetmore, D. R., Brouillette, C. G., and Hunt, J. F. (2010) Integrated biophysical studies implicate partial unfolding of NBD1 of CFTR in the molecular pathogenesis of F508del cystic fibrosis. *Protein Sci* **19**, 1932-1947
12. Higgins, C. F. (1992) ABC transporters: from microorganisms to man. *Annu Rev Cell Biol* **8**, 67-113
13. Gadsby, D. C., Vergani, P., and Csanady, L. (2006) The ABC protein turned chloride channel whose failure causes cystic fibrosis. *Nature* **440**, 477-483
14. Rich, D. P., Anderson, M. P., Gregory, R. J., Cheng, S. H., Paul, S., Jefferson, D. M., McCann, J. D., Klinger, K. W., Smith, A. E., and Welsh, M. J. (1990) Expression of cystic fibrosis transmembrane conductance regulator corrects defective chloride channel regulation in cystic fibrosis airway epithelial cells. *Nature* **347**, 358-363
15. Thibodeau, P. H., Brautigam, C. A., Machius, M., and Thomas, P. J. (2005) Side chain and backbone contributions of Phe508 to CFTR folding. *Nat Struct Mol Biol* **12**, 10-16
16. Lewis, H. A., Wang, C., Zhao, X., Hamuro, Y., Connors, K., Kearins, M. C., Lu, F., Sauder, J. M., Molnar, K. S., Coales, S. J., Maloney, P. C., Guggino, W. B., Wetmore, D. R., Weber, P. C., and Hunt, J. F. (2010) Structure and dynamics of NBD1 from CFTR characterized using crystallography and hydrogen/deuterium exchange mass spectrometry. *J Mol Biol* **396**, 406-430

17. Lewis, H. A., Zhao, X., Wang, C., Sauder, J. M., Rooney, I., Noland, B. W., Lorimer, D., Kearins, M. C., Conners, K., Condon, B., Maloney, P. C., Guggino, W. B., Hunt, J. F., and Emtage, S. (2005) Impact of the deltaF508 mutation in first nucleotide-binding domain of human cystic fibrosis transmembrane conductance regulator on domain folding and structure. *J Biol Chem* **280**, 1346-1353
18. Lewis, H. A., Buchanan, S. G., Burley, S. K., Conners, K., Dickey, M., Dorwart, M., Fowler, R., Gao, X., Guggino, W. B., Hendrickson, W. A., Hunt, J. F., Kearins, M. C., Lorimer, D., Maloney, P. C., Post, K. W., Rajashankar, K. R., Rutter, M. E., Sauder, J. M., Shriver, S., Thibodeau, P. H., Thomas, P. J., Zhang, M., Zhao, X., and Emtage, S. (2004) Structure of nucleotide-binding domain 1 of the cystic fibrosis transmembrane conductance regulator. *The EMBO journal* **23**, 282-293
19. Liu, F., Zhang, Z., Csanady, L., Gadsby, D. C., and Chen, J. (2017) Molecular Structure of the Human CFTR Ion Channel. *Cell* **169**, 85-95 e88
20. Serohijos, A. W., Hegedus, T., Aleksandrov, A. A., He, L., Cui, L., Dokholyan, N. V., and Riordan, J. R. (2008) Phenylalanine-508 mediates a cytoplasmic-membrane domain contact in the CFTR 3D structure crucial to assembly and channel function. *Proc Natl Acad Sci U S A* **105**, 3256-3261
21. Mornon, J. P., Lehn, P., and Callebaut, I. (2009) Molecular models of the open and closed states of the whole human CFTR protein. *Cell Mol Life Sci* **66**, 3469-3486
22. Corradi, V., Vergani, P., and Tieleman, D. P. (2015) Cystic Fibrosis Transmembrane Conductance Regulator (CFTR): CLOSED AND OPEN STATE CHANNEL MODELS. *J Biol Chem* **290**, 22891-22906
23. Rahman, K. S., Cui, G., Harvey, S. C., and McCarty, N. A. (2013) Modeling the conformational changes underlying channel opening in CFTR. *PLoS One* **8**, e74574
24. Gentzsch, M., Chang, X. B., Cui, L., Wu, Y., Ozols, V. V., Choudhury, A., Pagano, R. E., and Riordan, J. R. (2004) Endocytic trafficking routes of wild type and DeltaF508 cystic fibrosis transmembrane conductance regulator. *Mol Biol Cell* **15**, 2684-2696
25. Cheng, S. H., Gregory, R. J., Marshall, J., Paul, S., Souza, D. W., White, G. A., O'Riordan, C. R., and Smith, A. E. (1990) Defective intracellular transport and processing of CFTR is the molecular basis of most cystic fibrosis. *Cell* **63**, 827-834
26. Matsumura, Y., Sakai, J., and Skach, W. R. (2013) Endoplasmic reticulum protein quality control is determined by cooperative interactions between Hsp/c70 protein and the CHIP E3 ligase. *J Biol Chem* **288**, 31069-31079
27. Aleksandrov, A. A., Kota, P., Cui, L., Jensen, T., Alekseev, A. E., Reyes, S., He, L., Gentzsch, M., Aleksandrov, L. A., Dokholyan, N. V., and Riordan, J. R. (2012) Allosteric modulation balances thermodynamic stability and restores function of DeltaF508 CFTR. *J Mol Biol* **419**, 41-60
28. Du, K., Sharma, M., and Lukacs, G. L. (2005) The DeltaF508 cystic fibrosis mutation impairs domain-domain interactions and arrests post-translational folding of CFTR. *Nat Struct Mol Biol* **12**, 17-25
29. Rabeh, W. M., Bossard, F., Xu, H., Okiyoneda, T., Bagdany, M., Mulvihill, C. M., Du, K., di Bernardo, S., Liu, Y., Konermann, L., Roldan, A., and Lukacs, G. L. (2012) Correction of both NBD1 energetics and domain interface is required to restore DeltaF508 CFTR folding and function. *Cell* **148**, 150-163
30. Mendoza, J. L., Schmidt, A., Li, Q., Nuvaga, E., Barrett, T., Bridges, R. J., Feranchak, A. P., Brautigam, C. A., and Thomas, P. J. (2012) Requirements for efficient correction of DeltaF508 CFTR revealed by analyses of evolved sequences. *Cell* **148**, 164-174

31. He, L., Kota, P., Aleksandrov, A. A., Cui, L., Jensen, T., Dokholyan, N. V., and Riordan, J. R. (2013) Correctors of DeltaF508 CFTR restore global conformational maturation without thermally stabilizing the mutant protein. *FASEB J* **27**, 536-545
32. Loo, T. W., Bartlett, M. C., and Clarke, D. M. (2010) The V510D suppressor mutation stabilizes DeltaF508-CFTR at the cell surface. *Biochemistry* **49**, 6352-6357
33. He, L., Aleksandrov, L. A., Cui, L., Jensen, T. J., Nesbitt, K. L., and Riordan, J. R. (2010) Restoration of domain folding and interdomain assembly by second-site suppressors of the DeltaF508 mutation in CFTR. *FASEB J* **24**, 3103-3112
34. Pissarra, L. S., Farinha, C. M., Xu, Z., Schmidt, A., Thibodeau, P. H., Cai, Z., Thomas, P. J., Sheppard, D. N., and Amaral, M. D. (2008) Solubilizing mutations used to crystallize one CFTR domain attenuate the trafficking and channel defects caused by the major cystic fibrosis mutation. *Chem Biol* **15**, 62-69
35. DeCarvalho, A. C., Gansheroff, L. J., and Teem, J. L. (2002) Mutations in the nucleotide binding domain 1 signature motif region rescue processing and functional defects of cystic fibrosis transmembrane conductance regulator delta f508. *J Biol Chem* **277**, 35896-35905
36. Sato, S., Ward, C. L., Krouse, M. E., Wine, J. J., and Kopito, R. R. (1996) Glycerol reverses the misfolding phenotype of the most common cystic fibrosis mutation. *J Biol Chem* **271**, 635-638
37. Okiyoneda, T., Veit, G., Dekkers, J. F., Bagdany, M., Soya, N., Xu, H., Roldan, A., Verkman, A. S., Kurth, M., Simon, A., Hegedus, T., Beekman, J. M., and Lukacs, G. L. (2013) Mechanism-based corrector combination restores DeltaF508-CFTR folding and function. *Nat Chem Biol* **9**, 444-454
38. Freire, E. (2015) The Binding Thermodynamics of Drug Candidates. in *Thermodynamics and Kinetics of Drug Binding*, Wiley-VCH Verlag GmbH & Co. KGaA. pp 1-13
39. He, L., Aleksandrov, A. A., An, J., Cui, L., Yang, Z., Brouillette, C. G., and Riordan, J. R. (2015) Restoration of NBD1 thermal stability is necessary and sufficient to correct F508 CFTR folding and assembly. *J Mol Biol* **427**, 106-120
40. Sampson, H. M., Robert, R., Liao, J., Matthes, E., Carlile, G. W., Hanrahan, J. W., and Thomas, D. Y. (2011) Identification of a NBD1-binding pharmacological chaperone that corrects the trafficking defect of F508del-CFTR. *Chem Biol* **18**, 231-242
41. Aleksandrov, A. A., Kota, P., Aleksandrov, L. A., He, L., Jensen, T., Cui, L., Gentzsch, M., Dokholyan, N. V., and Riordan, J. R. (2010) Regulatory insertion removal restores maturation, stability and function of DeltaF508 CFTR. *J Mol Biol* **401**, 194-210
42. Lukacs, G. L., Mohamed, A., Kartner, N., Chang, X. B., Riordan, J. R., and Grinstein, S. (1994) Conformational maturation of CFTR but not its mutant counterpart (delta F508) occurs in the endoplasmic reticulum and requires ATP. *The EMBO journal* **13**, 6076-6086
43. Runnels, L. W., and Scarlata, S. F. (1995) Theory and application of fluorescence homotransfer to melittin oligomerization. *Biophys J* **69**, 1569-1583
44. Atwell, S., Brouillette, C. G., Connors, K., Emtage, S., Gheyi, T., Guggino, W. B., Hendle, J., Hunt, J. F., Lewis, H. A., Lu, F., Protasevich, II, Rodgers, L. A., Romero, R., Wasserman, S. R., Weber, P. C., Wetmore, D., Zhang, F. F., and Zhao, X. (2010) Structures of a minimal human CFTR first nucleotide-binding domain as a monomer, head-to-tail homodimer, and pathogenic mutant. *Protein Eng Des Sel* **23**, 375-384
45. Yin, S., Ding, F., and Dokholyan, N. V. (2007) Eris: an automated estimator of protein stability. *Nature methods* **4**, 466-467

46. Zhang, J. H., Chung, T. D., and Oldenburg, K. R. (1999) A Simple Statistical Parameter for Use in Evaluation and Validation of High Throughput Screening Assays. *Journal of biomolecular screening* **4**, 67-73
47. Dawson, R. J., and Locher, K. P. (2006) Structure of a bacterial multidrug ABC transporter. *Nature* **443**, 180-185
48. Hopfner, K. P., Karcher, A., Shin, D. S., Craig, L., Arthur, L. M., Carney, J. P., and Tainer, J. A. (2000) Structural biology of Rad50 ATPase: ATP-driven conformational control in DNA double-strand break repair and the ABC-ATPase superfamily. *Cell* **101**, 789-800
49. Anderson, M. P., Berger, H. A., Rich, D. P., Gregory, R. J., Smith, A. E., and Welsh, M. J. (1991) Nucleoside triphosphates are required to open the CFTR chloride channel. *Cell* **67**, 775-784
50. Aleksandrov, A. A., Aleksandrov, L., and Riordan, J. R. (2002) Nucleoside triphosphate pentose ring impact on CFTR gating and hydrolysis. *FEBS letters* **518**, 183-188
51. Aleksandrov, A. A., Cui, L., and Riordan, J. R. (2009) Relationship between nucleotide binding and ion channel gating in cystic fibrosis transmembrane conductance regulator. *J Physiol* **587**, 2875-2886
52. Bagdany, M., Veit, G., Fukuda, R., Avramescu, R. G., Okiyoneda, T., Baaklini, I., Singh, J., Sovak, G., Xu, H., Apaja, P. M., Sattin, S., Beitel, L. K., Roldan, A., Colombo, G., Balch, W., Young, J. C., and Lukacs, G. L. (2017) Chaperones rescue the energetic landscape of mutant CFTR at single molecule and in cell. *Nat Commun* **8**, 398
53. Meng, X., Wang, Y., Wang, X., Wrennall, J. A., Rimmington, T. L., Li, H., Cai, Z., Ford, R. C., and Sheppard, D. N. (2017) Two Small Molecules Restore Stability to a Subpopulation of the Cystic Fibrosis Transmembrane Conductance Regulator with the Predominant Disease-causing Mutation. *J Biol Chem* **292**, 3706-3719
54. Carson, M. R., Winter, M. C., Travis, S. M., and Welsh, M. J. (1995) Pyrophosphate stimulates wild-type and mutant cystic fibrosis transmembrane conductance regulator Cl<sup>-</sup> channels. *J Biol Chem* **270**, 20466-20472
55. Dong, Q., Ostedgaard, L. S., Rogers, C., Vermeer, D. W., Zhang, Y., and Welsh, M. J. (2012) Human-mouse cystic fibrosis transmembrane conductance regulator (CFTR) chimeras identify regions that partially rescue CFTR-DeltaF508 processing and alter its gating defect. *Proc Natl Acad Sci U S A* **109**, 917-922
56. Eckford, P. D., Ramjeesingh, M., Molinski, S., Pasyk, S., Dekkers, J. F., Li, C., Ahmadi, S., Ip, W., Chung, T. E., Du, K., Yeger, H., Beekman, J., Gonska, T., and Bear, C. E. (2014) VX-809 and related corrector compounds exhibit secondary activity stabilizing active F508del-CFTR after its partial rescue to the cell surface. *Chem Biol* **21**, 666-678
57. Hall, J. D., Wang, H., Byrnes, L. J., Shanker, S., Wang, K., Efremov, I. V., Chong, P. A., Forman-Kay, J. D., and Aulabaugh, A. E. (2016) Binding screen for cystic fibrosis transmembrane conductance regulator correctors finds new chemical matter and yields insights into cystic fibrosis therapeutic strategy. *Protein Sci* **25**, 360-373
58. Sampson, H. M., Lam, H., Chen, P. C., Zhang, D., Mottillo, C., Mirza, M., Qasim, K., Shrier, A., Shyng, S. L., Hanrahan, J. W., and Thomas, D. Y. (2013) Compounds that correct F508del-CFTR trafficking can also correct other protein trafficking diseases: an in vitro study using cell lines. *Orphanet J Rare Dis* **8**, 11
59. Liang, F., Kwok, I. S., Bhatt, P., Kaczmatek, S., Valdez, R., Layer, E., Fitzpatrick, R. J., and Kolodziej, A. F. (2012) Rdr-1: Correction and Interaction with Deltaf508-Nbd1. *Pediatr Pulm* **47**, 224-225

60. Van Goor, F., Hadida, S., Grootenhuys, P. D., Burton, B., Stack, J. H., Straley, K. S., Decker, C. J., Miller, M., McCartney, J., Olson, E. R., Wine, J. J., Frizzell, R. A., Ashlock, M., and Negulescu, P. A. (2011) Correction of the F508del-CFTR protein processing defect in vitro by the investigational drug VX-809. *Proc Natl Acad Sci U S A* **108**, 18843-18848
61. Pedemonte, N., Lukacs, G. L., Du, K., Caci, E., Zegarra-Moran, O., Galletta, L. J., and Verkman, A. S. (2005) Small-molecule correctors of defective DeltaF508-CFTR cellular processing identified by high-throughput screening. *J Clin Invest* **115**, 2564-2571
62. Chung, W. J., Goeckeler-Fried, J. L., Havasi, V., Chiang, A., Rowe, S. M., Plyler, Z. E., Hong, J. S., Mazur, M., Piazza, G. A., Keeton, A. B., White, E. L., Rasmussen, L., Weissman, A. M., Denny, R. A., Brodsky, J. L., and Sorscher, E. J. (2016) Increasing the Endoplasmic Reticulum Pool of the F508del Allele of the Cystic Fibrosis Transmembrane Conductance Regulator Leads to Greater Folding Correction by Small Molecule Therapeutics. *PLoS One* **11**, e0163615
63. Hudson, R. P., Dawson, J. E., Chong, P. A., Yang, Z., Millen, L., Thomas, P. J., Brouillette, C. G., and Forman-Kay, J. D. (2017) Direct Binding of the Corrector VX-809 to Human CFTR NBD1: Evidence of an Allosteric Coupling between the Binding Site and the NBD1:CL4 Interface. *Mol Pharmacol* **92**, 124-135
64. Pendergast, W., Yerxa, B. R., Douglass, J. G., 3rd, Shaver, S. R., Dougherty, R. W., Redick, C. C., Sims, I. F., and Rideout, J. L. (2001) Synthesis and P2Y receptor activity of a series of uridine dinucleoside 5'-polyphosphates. *Bioorg Med Chem Lett* **11**, 157-160
65. Vaccaro, J. A., Parnell, K. M., Terezakis, S. A., and Anderson, K. S. (2000) Mechanism of inhibition of the human immunodeficiency virus type 1 reverse transcriptase by d4TTP: an equivalent incorporation efficiency relative to the natural substrate dTTP. *Antimicrob Agents Chemother* **44**, 217-221
66. Fischer, J. n., and Ganellin, C. R. (2006) *Analogue-based drug discovery*, Wiley-VCH, Weinheim
67. Traut, T. W. (1994) Physiological concentrations of purines and pyrimidines. *Mol Cell Biochem* **140**, 1-22
68. Furman, P. A., Fyfe, J. A., St Clair, M. H., Weinhold, K., Rideout, J. L., Freeman, G. A., Lehrman, S. N., Bolognesi, D. P., Broder, S., Mitsuya, H., and et al. (1986) Phosphorylation of 3'-azido-3'-deoxythymidine and selective interaction of the 5'-triphosphate with human immunodeficiency virus reverse transcriptase. *Proc Natl Acad Sci U S A* **83**, 8333-8337
69. Elion, G. B., Furman, P. A., Fyfe, J. A., de Miranda, P., Beauchamp, L., and Schaeffer, H. J. (1977) Selectivity of action of an antiherpetic agent, 9-(2-hydroxyethoxymethyl) guanine. *Proc Natl Acad Sci U S A* **74**, 5716-5720
70. Eckhardt, B. J., and Gulick, R. M. (2017) 152 - Drugs for HIV Infection A2 - Cohen, Jonathan. in *Infectious Diseases (Fourth Edition)* (Powderly, W. G., and Opal, S. M. eds.), Elsevier. pp 1293-1308.e1292
71. Rakoczy, E. P., Kiel, C., McKeone, R., Stricher, F., and Serrano, L. (2011) Analysis of disease-linked rhodopsin mutations based on structure, function, and protein stability calculations. *J Mol Biol* **405**, 584-606
72. Ingram, V. M. (1957) Gene mutations in human haemoglobin: the chemical difference between normal and sickle cell haemoglobin. *Nature* **180**, 326-328
73. Sawaya, M. R., Sambashivan, S., Nelson, R., Ivanova, M. I., Sievers, S. A., Apostol, M. I., Thompson, M. J., Balbirnie, M., Wiltzius, J. J., McFarlane, H. T., Madsen, A. O., Riek, C., and Eisenberg, D. (2007) Atomic structures of amyloid cross-beta spines reveal varied steric zippers. *Nature* **447**, 453-457

74. Uversky, V. N., and Fink, A. L. (2006) *Protein misfolding, aggregation, and conformational diseases*, Springer Science+Business Media, New York, N.Y.
75. Valastyan, J. S., and Lindquist, S. (2014) Mechanisms of protein-folding diseases at a glance. *Dis Model Mech* **7**, 9-14
76. Ding, F., and Dokholyan, N. V. (2006) Emergence of protein fold families through rational design. *PLoS Comput Biol* **2**, e85
77. Dokholyan, N. V., Buldyrev, S. V., Stanley, H. E., and Shakhnovich, E. I. (1998) Discrete molecular dynamics studies of the folding of a protein-like model. *Fold Des* **3**, 577-587
78. Ding, F., Tsao, D., Nie, H., and Dokholyan, N. V. (2008) Ab initio folding of proteins with all-atom discrete molecular dynamics. *Structure* **16**, 1010-1018
79. Shirvanyants, D., Ding, F., Tsao, D., Ramachandran, S., and Dokholyan, N. V. (2012) Discrete molecular dynamics: an efficient and versatile simulation method for fine protein characterization. *J Phys Chem B* **116**, 8375-8382
80. Yin, S., Ding, F., and Dokholyan, N. V. (2007) Modeling backbone flexibility improves protein stability estimation. *Structure* **15**, 1567-1576
81. Moro, W. B., Yang, Z., Kane, T. A., Brouillette, C. G., and Brouillette, W. J. (2009) Virtual screening to identify lead inhibitors for bacterial NAD synthetase (NADs). *Bioorg Med Chem Lett* **19**, 2001-2005
82. Jelesarov, I., and Bosshard, H. R. (1999) Isothermal titration calorimetry and differential scanning calorimetry as complementary tools to investigate the energetics of biomolecular recognition. *Journal of Molecular Recognition* **12**, 3-18
83. Hassell, A. M., An, G., Bledsoe, R. K., Bynum, J. M., Carter, H. L., 3rd, Deng, S. J., Gampe, R. T., Grisard, T. E., Madauss, K. P., Nolte, R. T., Rocque, W. J., Wang, L., Weaver, K. L., Williams, S. P., Wisely, G. B., Xu, R., and Shewchuk, L. M. (2007) Crystallization of protein-ligand complexes. *Acta Crystallogr D Biol Crystallogr* **63**, 72-79
84. Otwinowski, Z., and Minor, W. (1997) Processing of X-ray diffraction data collected in oscillation mode. *Method Enzymol* **276**, 307-326
85. Adams, P. D., Afonine, P. V., Bunkoczi, G., Chen, V. B., Davis, I. W., Echols, N., Headd, J. J., Hung, L. W., Kapral, G. J., Grosse-Kunstleve, R. W., McCoy, A. J., Moriarty, N. W., Oeffner, R., Read, R. J., Richardson, D. C., Richardson, J. S., Terwilliger, T. C., and Zwart, P. H. (2010) PHENIX: a comprehensive Python-based system for macromolecular structure solution. *Acta Crystallogr D Biol Crystallogr* **66**, 213-221
86. Aleksandrov, L., Aleksandrov, A. A., Chang, X. B., and Riordan, J. R. (2002) The first nucleotide binding domain of cystic fibrosis transmembrane conductance regulator is a site of stable nucleotide interaction, whereas the second is a site of rapid turnover. *Journal of Biological Chemistry* **277**, 15419-15425
87. Aleksandrov, L., Mengos, A., Chang, X. B., Aleksandrov, A., and Riordan, J. R. (2001) Differential interactions of nucleotides at the two nucleotide binding domains of the cystic fibrosis transmembrane conductance regulator. *Journal of Biological Chemistry* **276**, 12918-12923
88. Bompadre, S. G., Cho, J. H., Wang, X., Zou, X., Sohma, Y., Li, M., and Hwang, T. C. (2005) CFTR gating II: Effects of nucleotide binding on the stability of open states. *J Gen Physiol* **125**, 377-394
89. Zhou, Z., Wang, X., Li, M., Sohma, Y., Zou, X., and Hwang, T. C. (2005) High affinity ATP/ADP analogues as new tools for studying CFTR gating. *J Physiol* **569**, 447-457

90. Bompadre, S. G., Ai, T., Cho, J. H., Wang, X., Sohma, Y., Li, M., and Hwang, T. C. (2005) CFTR gating I: Characterization of the ATP-dependent gating of a phosphorylation-independent CFTR channel (DeltaR-CFTR). *J Gen Physiol* **125**, 361-375
91. Ostedgaard, L. S., Baldursson, O., Vermeer, D. W., Welsh, M. J., and Robertson, A. D. (2000) A functional R domain from cystic fibrosis transmembrane conductance regulator is predominantly unstructured in solution. *Proc Natl Acad Sci U S A* **97**, 5657-5662
92. Baker, J. M., Hudson, R. P., Kanelis, V., Choy, W. Y., Thibodeau, P. H., Thomas, P. J., and Forman-Kay, J. D. (2007) CFTR regulatory region interacts with NBD1 predominantly via multiple transient helices. *Nat Struct Mol Biol* **14**, 738-745
93. Kanelis, V., Hudson, R. P., Thibodeau, P. H., Thomas, P. J., and Forman-Kay, J. D. (2010) NMR evidence for differential phosphorylation-dependent interactions in WT and DeltaF508 CFTR. *The EMBO journal* **29**, 263-277
94. Griko, Y. V., Privalov, P. L., Venyaminov, S. Y., and Kutysenko, V. P. (1988) Thermodynamic Study of the Apomyoglobin Structure. *Journal of Molecular Biology* **202**, 127-138
95. Privalov, P. L. (1989) Thermodynamic problems of protein structure. *Annu Rev Biophys Biophys Chem* **18**, 47-69
96. Jeng, M. F., Englander, S. W., Elove, G. A., Wand, A. J., and Roder, H. (1990) Structural description of acid-denatured cytochrome c by hydrogen exchange and 2D NMR [published erratum appears in *Biochemistry* 1991 Mar 19;30(11):2988]. *Biochemistry* **29**, 10433-10437
97. Ptitsyn, O. B., Pain, R. H., Semisotnov, G. V., Zerovnik, E., and Razgulyaev, O. I. (1990) Evidence for a Molten Globule State as a General Intermediate in Protein Folding. *FEBS letters* **262**, 20-24
98. Baldwin, R. L. (1991) Experimental studies of pathways of protein folding. *Ciba Found Symp* **161**, 190-201; discussion 201-195
99. Hughson, F. M., Barrick, D., and Baldwin, R. L. (1991) Probing the stability of a partly folded apomyoglobin intermediate by site-directed mutagenesis. *Biochemistry* **30**, 4113-4118
100. Barrick, D., and Baldwin, R. L. (1993) Stein and Moore Award address. The molten globule intermediate of apomyoglobin and the process of protein folding. *Protein Sci* **2**, 869-876
101. Dobson, C. M. (1994) Protein folding. Solid evidence for molten globules. *Curr Biol* **4**, 636-640
102. Yin, S., Proctor, E. A., Lugovskoy, A. A., and Dokholyan, N. V. (2009) Fast screening of protein surfaces using geometric invariant fingerprints. *Proc Natl Acad Sci U S A* **106**, 16622-16626
103. Yin, S., Ding, F., and Dokholyan, N. V. (2010) Computational evaluation of protein stability change upon mutations. *Methods Mol Biol* **634**, 189-201
104. John, D. M., and Weeks, K. M. (2000) van't Hoff enthalpies without baselines. *Protein Sci* **9**, 1416-1419
105. Boyle, M. P., Bell, S. C., Konstan, M. W., McColley, S. A., Rowe, S. M., Rietschel, E., Huang, X., Waltz, D., Patel, N. R., Rodman, D., and group, V. X. s. (2014) A CFTR corrector (lumacaftor) and a CFTR potentiator (ivacaftor) for treatment of patients with cystic fibrosis who have a phe508del CFTR mutation: a phase 2 randomised controlled trial. *Lancet Respir Med* **2**, 527-538
106. Aleksandrov, L. A., Jensen, T. J., Cui, L., Kousouros, J. N., He, L., Aleksandrov, A. A., and Riordan, J. R. (2015) Thermal stability of purified and reconstituted CFTR in a locked open channel conformation. *Protein Expr Purif* **116**, 159-166

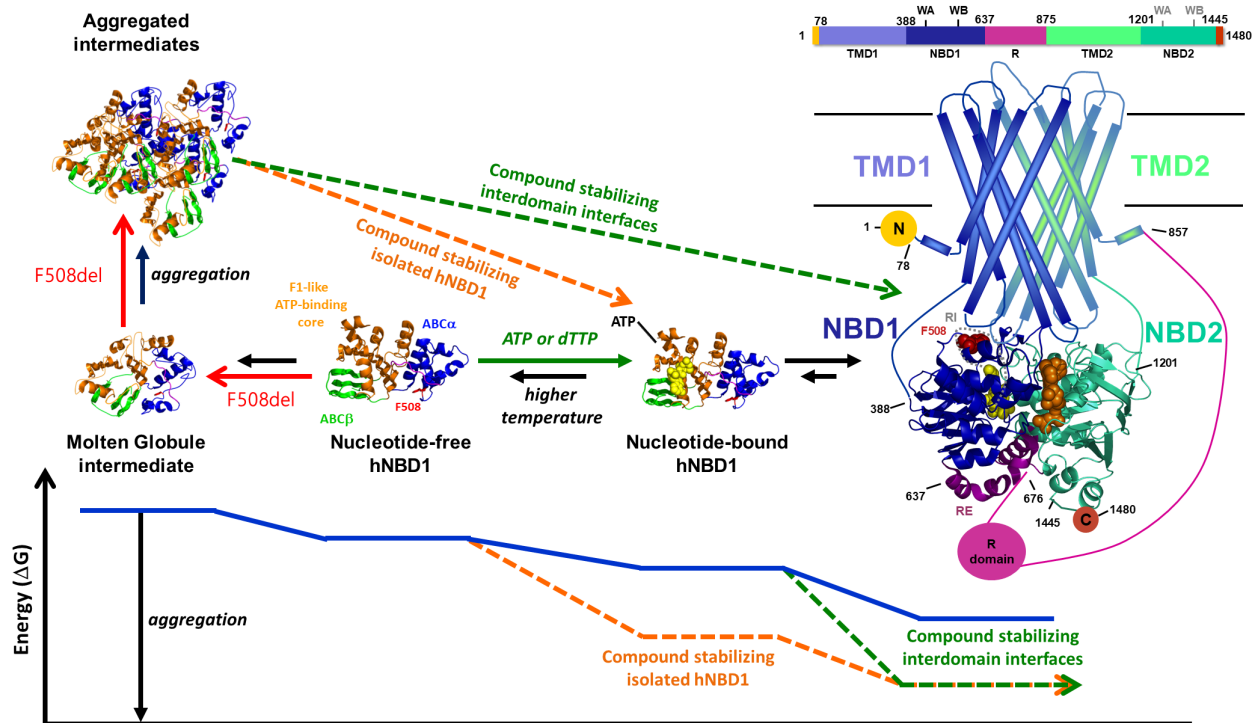


Figure 1. *Thermodynamic strategies to correct the disease-causing stability defect in F508del-CFTR.* The structure of human CFTR (hCFTR) is schematized at upper right. Its two nucleotide-binding domains, NBD1 (16-18,44) (blue, PDB id 2BBO) and NBD2 (green, PDB id 3GD7) bind two molecules of Mg-ATP (yellow and orange) at their mutual interface (4-11). Its two transmembrane domains, TMD1 (blue) and TMD2 (green) structurally interdigitate to form two composite binding sites (20,21), one for NBD1 and the other for NBD2. The Residue F508 (red), which is deleted in F508del-hCFTR is located on the surface of NBD1 that binds to the cognate binding site formed by TMD1/TMD2 (1,17,18,20,21). The regulatory or R region (magenta) is believed to be predominantly disordered but to have segments that reversibly bind to the other domains in hCFTR to modulate their behavior (16,91-93). The folding pathway of human NBD1 (hNBD1) is schematized in the center and at the left, above a free-energy diagram. The native conformation of hNBD1, which is stabilized by binding to ATP and the TMDs of hCFTR, is in equilibrium with a low energy "molten globule" conformation (94-101), which retains native-like secondary structure. Formation of this molten-globule species is inhibited by a wide range of second-site mutations (10,11,16) that also suppress the trafficking defect (32,34,41) in F508del-hCFTR that is responsible for causing cystic fibrosis (24). These observations support the hypothesis that the F508del mutation causes the disease by promoting formation of the highly aggregation-prone molten-globule intermediate. Thermodynamic theory suggests that chemical compounds that bind to F508del-hNBD1, either alone or at its interface with the TMDs of hCFTR, should pull the domain away from the molten globule conformation (20,27-30) and thereby offset the defect caused by the mutation (orange and green dotted lines in the free-energy diagram). This thermodynamic effect can be thought of as a form of "mass action".

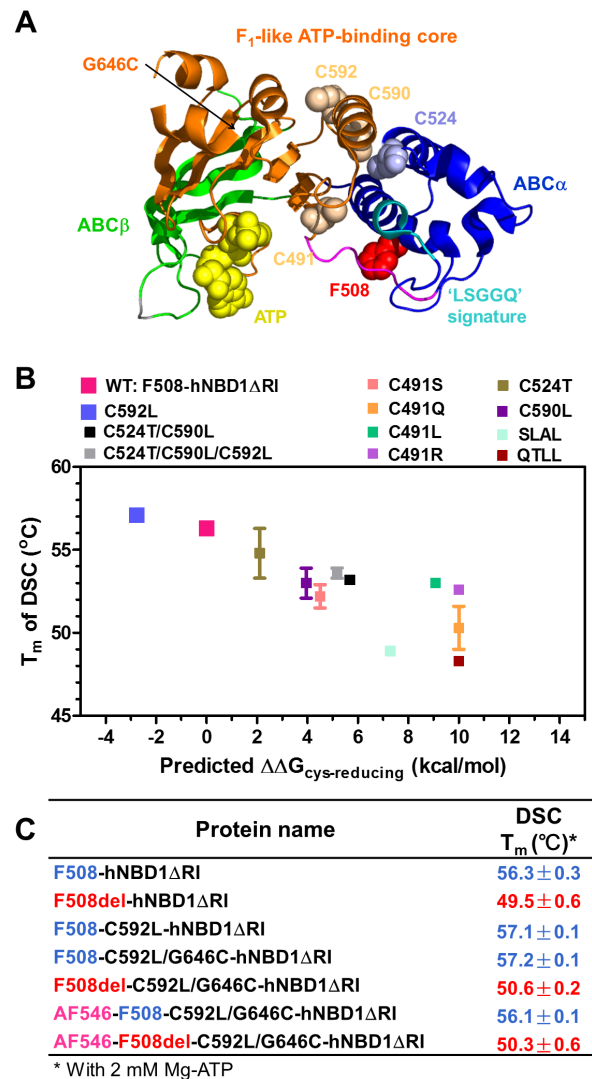


Figure 2. *Engineering hNBD1 for single site fluorescent labeling.* (A) Ribbon diagram of hNBD1ΔRI with Mg-ATP (yellow), residue F508 (red), and all cysteine (cys) residues in the native domain shown in space-filling representation. The cys residues are colored like the protein backbone in the subdomain in which they are located (orange for the F1-like ATP binding core, green for the ABCβ subdomain, and blue for the ABCα subdomain. PDB id 2PZE). (B) The melting temperature ( $T_m$ ) from differential scanning calorimetry (DSC) assays plotted against the change in the free energy of folding predicted by the program Eris (45,80,102,103) for 11 cys-reduced hNBD1ΔRI variants. Assays were conducted at 0.5 mg/mL protein using 2 mM ATP in Standard Stabilizing Buffer (SSB) containing 3 mM MgCl<sub>2</sub>, 150 mM NaCl, 10% (v/v) glycerol, 10% (v/v) ethylene glycol, 1 mM TCEP, and 20 mM Na-HEPES, pH 7.5. (C) Table showing the average value and sample variance of the  $T_m$  from at least two replicate DSC assays conducted in the same ATP-containing buffer on protein constructs used to develop or implement the fluorescence self-quenching assay for hNBD1ΔRI stability (Figure 3). The magenta prefix AF546- indicates protein covalently labeled with the fluorescent dye Alexa Fluor 546.

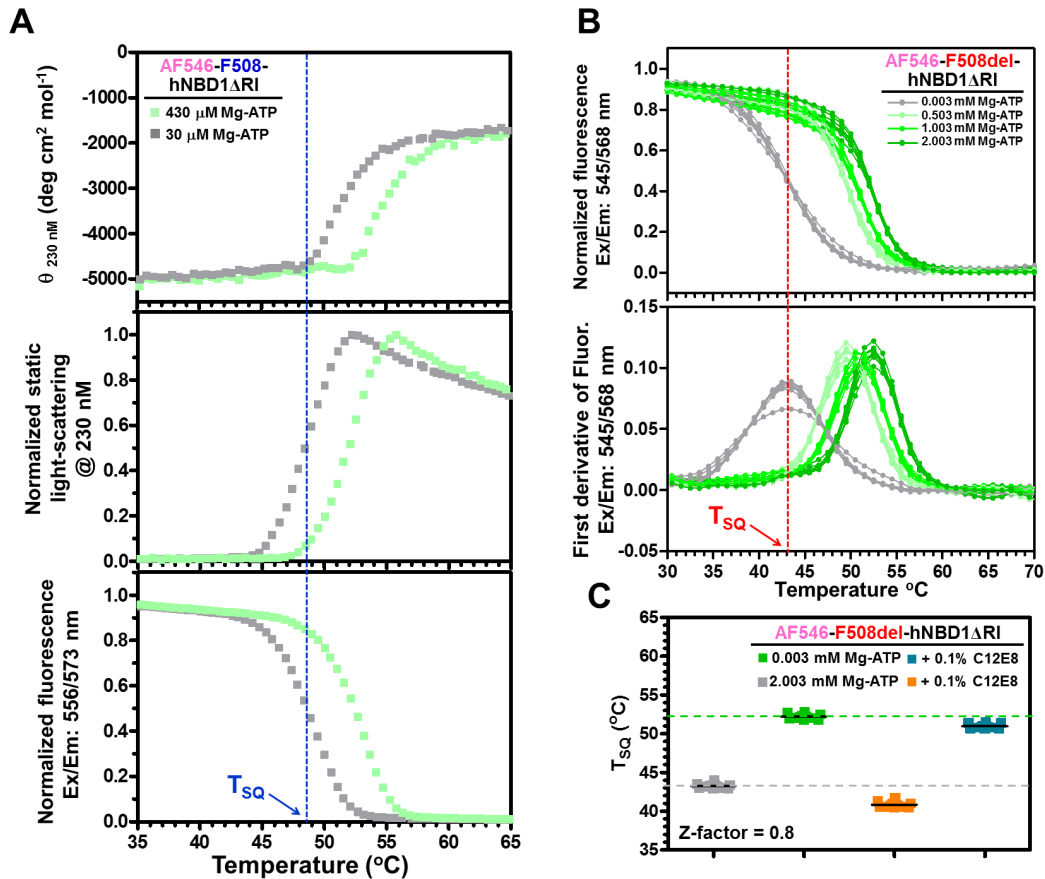


Figure 3. *Efficient thermal fluorescence self-quenching (tFSQ) assay for hNBD1 stability.* (A) Triple detection experiment monitoring far-UV circular dichroism (CD) at 230 nm (top), static light-scattering (SLS) at 230 nm (middle), and fluorescence emission intensity at 573 nm (bottom) during thermal denaturation at 3 °/min of 0.05 mg/mL (2  $\mu$ M) AF546-labeled F508-C592L/G646C-hNBD1 $\Delta$ RI in the presence of 30  $\mu$ M or 430  $\mu$ M Mg-ATP. The temperature corresponding to the steepest slope of decline in emission intensity, as determined using nonlinear curve fitting to the first derivative of the van't Hoff equation (104), is defined as the fluorescence self-quenching temperature ( $T_{SQ}$ ). These experiments were conducted as previously described (10,11) in a 1.6 ml cuvette using a fluorescence excitation wavelength of 556 nm. (B) Fluorescence emission intensity at 586 nm (top) and the first derivative of that intensity (bottom) during thermal denaturation of 0.005 mg/mL (~0.2  $\mu$ M) AF546-labeled F508del-C592L/G646C-hNBD1 $\Delta$ RI in a 10  $\mu$ L volume in a 96-well microtiter plate. Fluorescence in all wells was monitored in parallel using a real-time PCR machine with 545 nm excitation. Results are shown from three replicate assays conducted at each of four different Mg-ATP concentrations indicated on the graph. The  $T_{SQ}$  values here differ from panel A because the experiments employed different protein constructs (F508 vs. F508del) and ATP concentrations. (C)  $T_{SQ}$  values measured in eight replicate assays on AF546-labeled F508del-C592L/G646C-hNBD1 $\Delta$ RI conducted using the same methods in 3  $\mu$ M or 2,003  $\mu$ M Mg-ATP in the absence (left) or presence (right) of a 0.1% (w/v) concentration of the non-ionic detergent C12E8 (~10 $\times$ cmc). All assays in panels a-c were conducted in SSB.

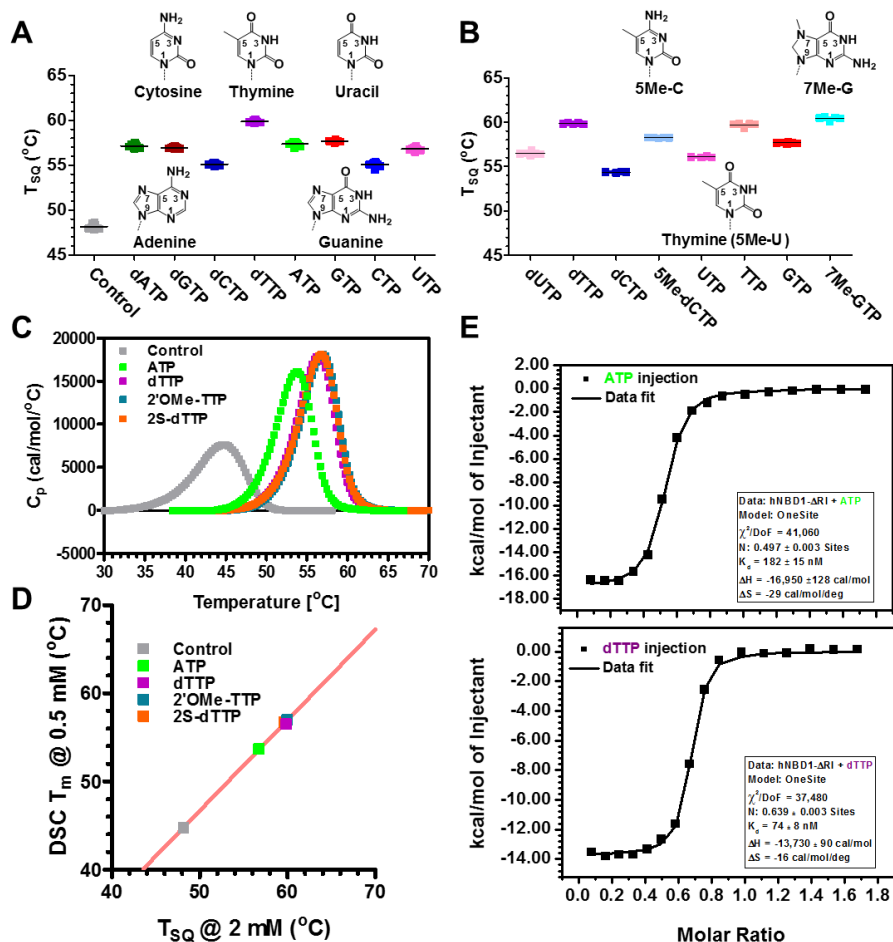


Figure 4. *Stabilization of hNBD1ΔRI by nucleotide analogs.* (A-B)  $T_{SQ}$  values from five replicate tFSQ assays conducted on AF546-labeled F508-C592L/G646C-hNBD1ΔRI in the presence of a 2 mM concentration of the  $Mg^{++}$  complex of the indicated nucleotide. The control assays contained 3  $\mu M$  Mg-ATP, which comes from the protein storage buffer and is present in all samples in addition to any added nucleotide. Assays were conducted in SSB using a heating rate of 3 °/min in a microtiter plate as in Figure 3B-C. Equivalent differences in  $T_{SQ}$  are observed in assays conducted with AF546-labeled F508del-C592L/G646C-hNBD1ΔRI (Figure S3B) or full-length C592L-hNBD1 (with native C647) retaining the RI and RE (Figure S3C-D). Sample variance for these assays ranged from 0.1-0.3°, as reported in Figure S5B. Data from four nucleotides are repeated panels A and B to illustrate the consistent effect of adding an exocyclic methyl group to the bases. (C) DSC assays conducted on 0.5 mg/mL protein in the presence of a 0.5 mM concentration of the  $Mg^{++}$  complex of the indicated nucleotide in SSB. (D) The  $T_m$  from DSC assays plotted against the  $T_{SQ}$  from the fluorescence self-quenching assays in Figure 4, which were conducted in the same buffer containing a higher 2 mM concentration of the  $Mg^{++}$  complexes of the indicated nucleotides. Linear regression gives a slope of  $1.03 \pm 0.02$  (red line). (E) Results from isothermal titration calorimetry (ITC) measurements of binding of ATP or dTTP to hNBD1ΔRI in the same buffer at 10 °C. The fitted binding stoichiometry likely reflects some aggregated protein that does not bind nucleotide, which should not perturb inferred thermodynamic parameters, as explained in the Materials and Methods section.

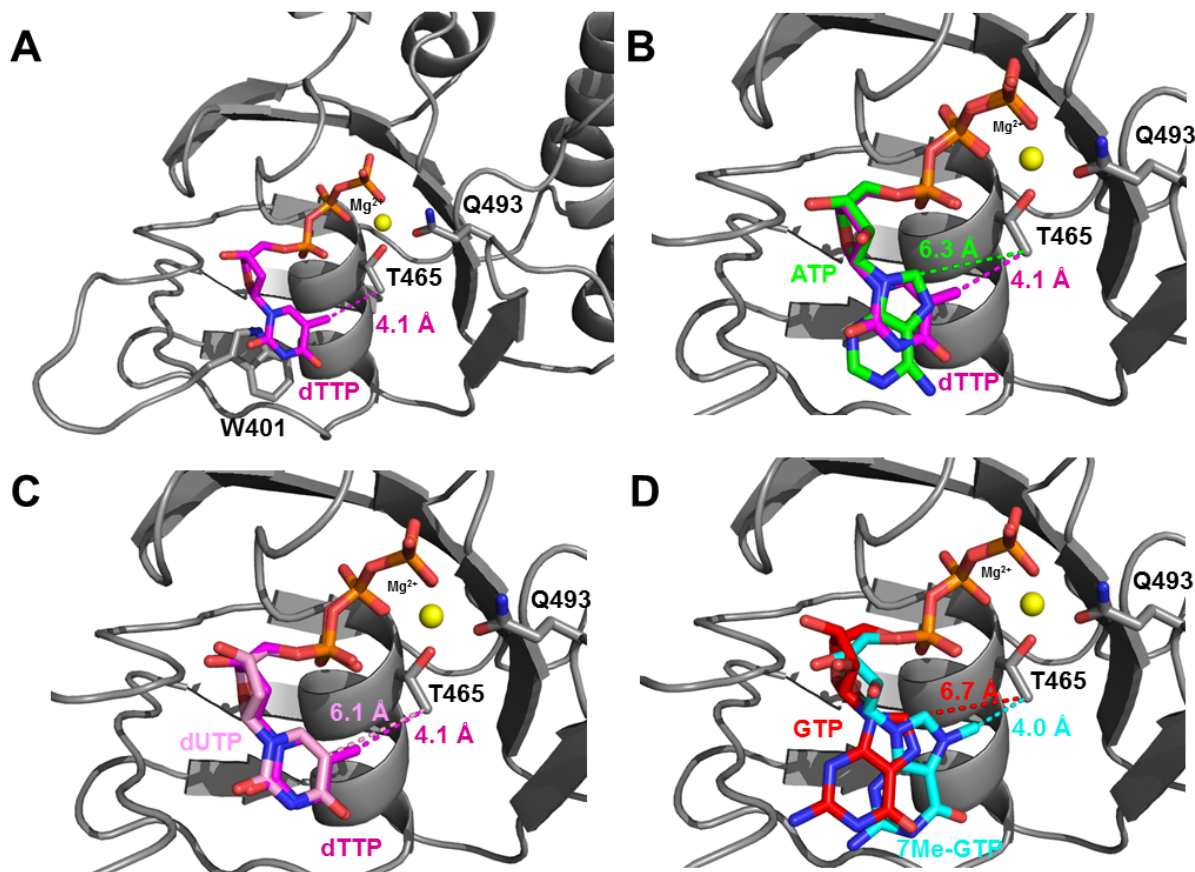


Figure 5 *X-ray crystal structures of nucleotides bound to hNBD1ΔRI.* (A-D) nucleotide-hNBD1ΔRI structures are in a tetragonal lattice in which the nucleotides do not participate in crystal-packing. The protein backbone and carbon atoms in two residues from the dTTP structure are shown in gray. The  $Mg^{++}$  cofactor bound to dTTP is shown as a yellow sphere. Four nucleotides from different structures are shown in ball-and-stick representation with carbon atoms colored according to nucleotide identity: magenta for dTTP (PDB id 5TF8,  $R_{free} = 18.7\%$  @ 1.86 Å), green for ATP (PDB id 5TF7,  $R_{free} = 20.0\%$  @ 1.93 Å), cyan for 7Me-GTP (PDB id 5TFB,  $R_{free} = 19.9\%$  @ 1.87 Å), pink for dUTP (PDB id 5TFA,  $R_{free} = 19.6\%$  @ 1.87 Å), and ruby for GTP (PDB id 5TFC,  $R_{free} = 20.2\%$  @ 1.92 Å). Oxygen, nitrogen, and phosphorous atoms are colored red, blue, and orange, respectively. Dotted lines connect atoms for which internuclear distances are given.

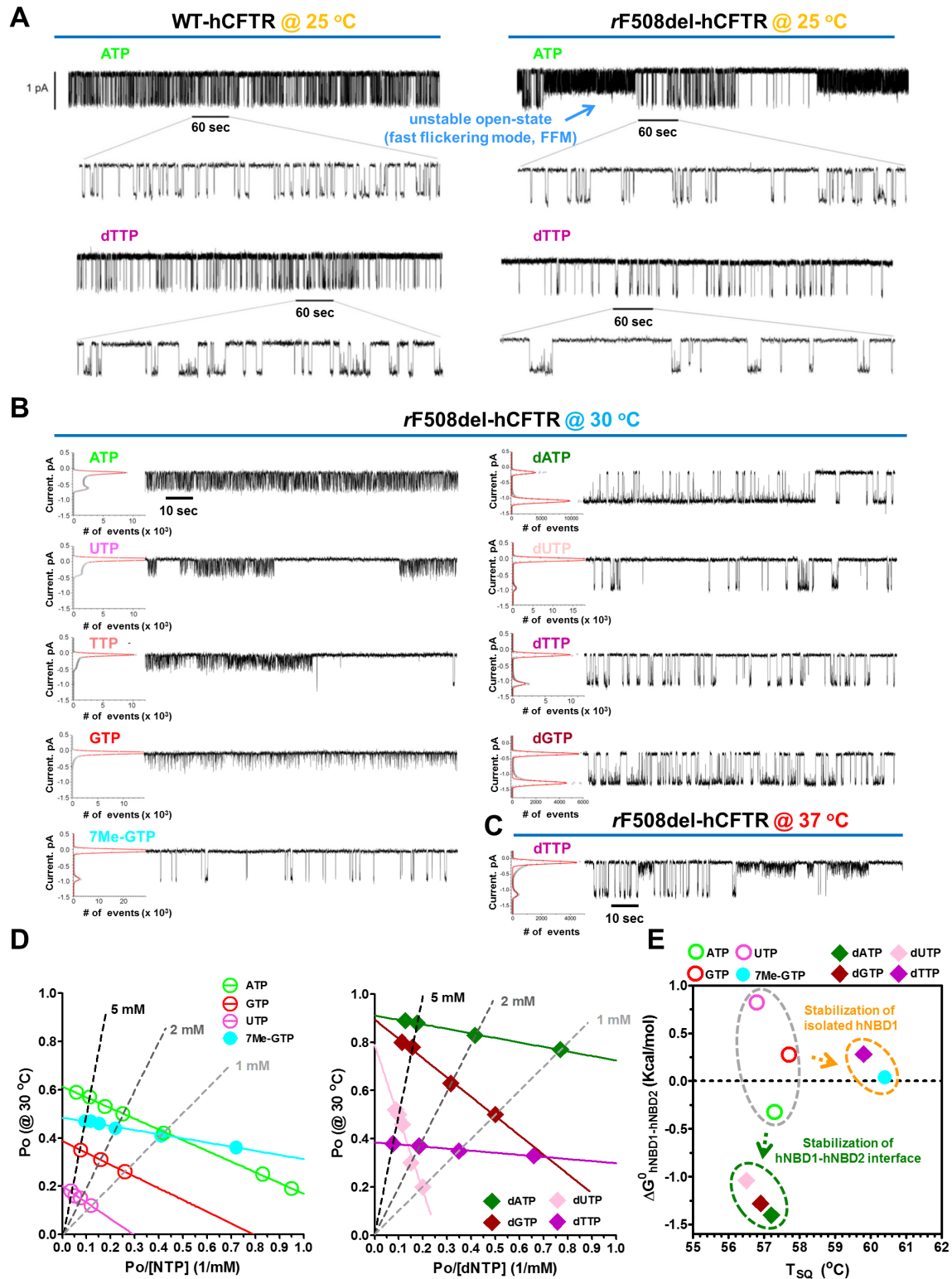


Figure 6. Temperature-dependent single-channels electrophysiology analyses of full-length hCFTR. (A-C) Single-channel electrophysiology measurements conducted at the indicated temperatures on wild-type (WT) hCFTR or VX809-rescued (105) F508del-hCFTR (rF508del-hCFTR) in the presence of the indicated nucleotide triphosphates (NTPs) at 2 mM concentration. Measurements were performed at 25 °C (panel A),

30 °C (panel B), or 37 °C (panel C) on proteins reconstituted into black lipid membranes (39,106). Electrical current is calibrated in picoamps (pA), and time is indicated in seconds (sec). The plots on the left in panels B-C show all-points histograms with the observed current on the ordinate, which were used to calculate channel open probability ( $P_o$ ). The lower expanded traces in panel A show 60 sec segments from the upper traces, which were recorded for 10 min, while the traces in panel B represent the final 2 min of a 20 min recording under each condition. Three different experiments of 10 min duration were used to calculate the single-channel parameters for both WT and rF058del-hCFTR at 25 °C in the presence of 2 mM dTTP:  $\gamma_{WT} = \gamma_{rF508del} = 10.6 \pm 0.1$  pS,  $P_{o-WT} = 0.15 \pm 0.02$ , and  $P_{o-rF08del} = 0.10 \pm 0.02$ . (D) Eadie-Hofstee-like plots showing  $P_o$  vs. ( $P_o/[NTP]$ ) values derived from electrophysiology experiments like those in panels A-C conducted at 30 °C on WT-hCFTR at varying concentrations of the indicated NTPs (raw data not shown). The slopes of the solid lines are proportional to the effective nucleotide dissociation constant or affinity in the open state of the channel, as described by the parameter  $K_{eff}$  in the Eadie-Hofstee equation presented in the text. The dotted lines connect points from experiments conducted at the same concentration of different nucleotides. At least five different experiments of 2 min duration were used to calculate the mean  $P_o$  value of for each NTP type and concentration. The values of the standard error of the mean are less than the size of the symbols and therefore not shown. (E) The Gibbs free energy change for opening the WT-hCFTR channel at saturating nucleotide concentration ( $\Delta G^0_{hNBD1-hNBD2}$ ) plotted against the fluorescence self-quenching temperature ( $T_{SQ}$ ) of F508-C592L/G646C-hNBD1 $\Delta$ RI at a 2 mM concentration of the same nucleotide (from Figures 4A-B). The value of  $\Delta G^0_{hNBD1-hNBD2}$  is calculated as  $-RT \cdot \ln(P_{o-max}/(1-P_{o-max}))$ . Decreasing  $\Delta G^0_{hNBD1-hNBD2}$  reflects greater stabilization of the functional hNBD1-hNBD2 interface, which is required for stable channel opening, whereas increasing  $T_{SQ}$  reflects greater stabilization of hNBD1 itself. Closed symbols are used for nucleotides that maintain normal activity of F508del-hCFTR channels at 30 °C, and open symbols are used for those that do not. The ellipses highlight the correlation predicted by the thermodynamic scheme in Figure 1 between the ability of nucleotides to rescue the thermal defect caused by the F508del mutation (panels B-C) and their efficacy in stabilizing either hNBD1 itself (orange dotted lines here and in Figure 1) or the hNBD1-hNBD2 interface (green dotted lines here and in Figure 1).

**Ligand binding to a remote site thermodynamically corrects the F508del mutation in the human cystic fibrosis transmembrane conductance regulator**

Chi Wang, Andrei A Aleksandrov, Zhengrong Yang, Farhad Forouhar, Elizabeth A. Proctor, Pradeep Kota, Jianli An, Anna Kaplan, Netaly Khazanov, Grégory Boël, Brent R Stockwell, Hanoch Senderowitz, Nikolay V. Dokholyan, John R. Riordan, Christie G. Brouillette and John F Hunt

*J. Biol. Chem.* published online June 14, 2018

---

Access the most updated version of this article at doi: [10.1074/jbc.RA117.000819](https://doi.org/10.1074/jbc.RA117.000819)

Alerts:

- [When this article is cited](#)
- [When a correction for this article is posted](#)

[Click here](#) to choose from all of JBC's e-mail alerts

*Supplementary Information*  
*for*

**Ligand binding to a remote site in the mutated domain thermodynamically corrects the stability defect caused by the F508del mutation in the human cystic fibrosis transmembrane conductance regulator**

**Authors:** Chi Wang<sup>1</sup>, Andrei A. Aleksandrov<sup>2†</sup>, Zhengrong Yang<sup>3†</sup>, Farhad Forouhar<sup>1§</sup>, Elizabeth A. Proctor<sup>2§</sup>, Pradeep Kota<sup>2§</sup>, Jianli An<sup>3</sup>, Anna Kaplan<sup>1</sup>, Netaly Khazanov<sup>4</sup>, Grégory Boël<sup>1§</sup>, Brent R. Stockwell<sup>1,5</sup>, Hanoch Senderowitz<sup>4</sup>, Nikolay V. Dokholyan<sup>2</sup>, John R. Riordan<sup>2</sup>, Christie G. Brouillette<sup>3</sup>, John F. Hunt<sup>1\*</sup>

**Affiliations:** <sup>1</sup> Department of Biological Sciences, Columbia University, New York, NY 10027, USA; <sup>2</sup> Department of Biochemistry and Biophysics, School of Medicine, University of North Carolina, Chapel Hill, NC 27599, USA; <sup>3</sup> Department of Chemistry, University of Alabama, Birmingham, AL 35294, USA; <sup>4</sup> Department of Chemistry, Bar-Ilan University, Ramat-Gan, 5290002, Israel; <sup>5</sup> Department of Chemistry, Columbia University, New York, NY 10027, USA.

† Authors who contributed equally

\*To whom correspondence should be addressed: Professor John F. Hunt Department of Biological Sciences, Columbia University, New York, NY 10027 (212)-854-5443*voice*; (212)-865-8246*FAX*; E-mail: [jfh21@columbia.edu](mailto:jfh21@columbia.edu).

**Running title:** *Thermodynamic correction of F508del-CFTR*

## Materials

*Materials.* Nucleotides were purchased from Sigma-Aldrich, St. Louis, MO (ADP, AMP, TDP, TMP, 7Me-GTP), Trilink Biotechnologies, San Diego, CA (2'OMe-TTP, TTP, 2S-dTTP, 3'-AM-ddTTP, 5Me-dCTP, 2'-AZ-dATP, 5-propynyl-dUTP, 5-FI-dUTP, 5-HMD-dUTP, and 5-AA-2'-dUTP), Sierra Bioresearch, Tucson, AZ (d4TTP), BIOLOG Life Science Institute, Bremen, Germany (6-PhEt-ATP (1)), AnaSpec, Fremont, CA (MANT-ATP), and Thermo-Fisher, Waltham, MA (ATP, GTP, CTP, UTP, dATP, dGTP, dCTP, dTTP, and dUTP). Ni-NTA resin, AlexaFluor546 maleimide, 2-mercaptoethanol, Imidazole, and Pierce BCA kit were purchased from Thermo-Fisher, Waltham, MA. Protease inhibitors were purchased from AG Scientific, San Diego, CA (Leupeptin, Aprotinin, Benzamidine, AEBSF, and E64). Compound VX809 was purchased from Selleck Chemicals, Houston, TX. Compound 5-(4-nitrophenyl)-2-furaldehyde 2-phenylhydrazine (RDR1) was purchased from Maybridge, Altrincham, UK. Lipids were purchased from Avanti Polar Lipids, Alabaster, AL (1-palmitoyl-2-oleoyl-sn-glycero-3-phosphoethanolamine and 1-palmitoyl-2-oleoyl-snglycero-3-phosphoserine). PKA catalytic subunit was purchased from Promega, Madison, WI. PD-10 desalting column and Sephacryl S200 resin were purchased from GE Healthcare, Pittsburgh, PA. PCR plates were purchased from USA Scientific, Orlando, FL (96-well and 384-well plates). Amicon centrifugal filters were purchased from EMD Millipore, Billerica, MA. Microbatch 72-well plate, 100% paraffin oil, and CrystalCap HT™ (SPINE) were purchased from Hampton Research, Aliso Viejo, CA.

*Buffers.* Standard Stabilizing Buffer (SSB) containing 150 mM NaCl, 10% (v/v) glycerol, 10% (v/v) ethylene glycol, 1 mM TCEP (tris(2-carboxymethyl) phosphine), 4 mM MgCl<sub>2</sub>, 2 mM ATP, and 20 mM Na-HEPES, pH 7.5. Hypotonic lysis buffer contains 1 mM EDTA, 5 mM ATP, 2 µg/mL leupeptin, 4 µg/mL aprotinin, 250 µg/mL benzamidine, 100 µg/mL AEBSF, 7 µg/mL E64, and 10 mM HEPES pH 7.2. Sucrose Buffer contains 500 mM sucrose, 5 mM ATP, 10 mM HEPES pH 7.2. Phosphorylation buffer contains 0.5 mM EGTA, 5 mM ATP, 5 mM MgCl<sub>2</sub>, and 250 mM sucrose 10mM HEPES pH 7.2. Symmetrical Salt Solution contains 3 mM MgCl<sub>2</sub>, 1 mM EGTA, and 300 mM Tris-HCl pH 7.2.

Table S1. ITC analyses on nucleotide analog binding to F508-hNBD1ΔRI.

Compounds	Stoichiometry (N) <sup>[b]</sup>	K <sub>d</sub> (μM)	ΔG (kcal/mol)	ΔH (kcal/mol)	ΔS (cal/mol/°C)	T•ΔS (kcal/mol) <sup>[c]</sup>	T <sub>sq</sub> (°C)
Uridine triphosphate (UTP) <sup>[a]</sup>	0.43 ± 0.02	0.51 ± 0.04	-8.0 ± 0.2	-16.9 ± 0.2	-31.3 ± 0.1	-8.86 ± 0.03	56.8 ± 0.2
Deoxyuridine triphosphate (dUTP) <sup>[a]</sup>	0.51 ± 0.05	0.84 ± 0.15	-7.9 ± 0.1	-13.1 ± 0.7	-18.0 ± 2.0	-5.09 ± 0.57	56.5 ± 0.2
Thymidine triphosphate (dTTP) <sup>[a]</sup>	0.58 ± 0.06	0.10 ± 0.03	-9.1 ± 0.2	-12.8 ± 0.7	-13.0 ± 2.0	-3.68 ± 0.57	59.8 ± 0.1
2-Thiothymidine Triphosphate (2S-dTTP) <sup>[a]</sup>	0.62 ± 0.03	0.10 ± 0.04	-9.1 ± 0.3	-13.0 ± 0.5	-14.0 ± 3.0	-3.96 ± 0.85	59.6 ± 0.1
2'-O-Methyl-5-methyluridine-5'-Triphosphate(2'OMe-TTP) <sup>[a]</sup>	0.42 ± 0.01	0.07 ± 0.02	-9.3 ± 0.2	-17.3 ± 0.6	-28.0 ± 2.0	-7.92 ± 0.57	60.0 ± 0.2
Adenosine triphosphate (ATP) <sup>[a]</sup>	0.47 ± 0.02	0.23 ± 0.03	-8.6 ± 0.1	-17.0 ± 0.2	-29.6 ± 0.9	-8.38 ± 0.26	57.3 ± 0.2
Deoxyadenosine triphosphate (dATP) <sup>[a]</sup>	0.49 ± 0.01	0.60 ± 0.10	-8.1 ± 0.1	-13.7 ± 0.1	-19.8 ± 0.1	-5.60 ± 0.03	57.2 ± 0.1
7-Methyl-Guanosine triphosphate(7Me-GTP) <sup>[a]</sup>	0.54 ± 0.01	0.20 ± 0.01	-8.7 ± 0.1	-17.1 ± 0.2	-29.5 ± 0.6	-8.35 ± 0.17	60.6 ± 0.2
Guanosine triphosphate (GTP) <sup>[a]</sup>	0.41 ± 0.01	0.21 ± 0.04	-8.7 ± 0.1	-17.4 ± 1.9	-30.7 ± 7.1	-8.69 ± 2.0	57.7 ± 0.1
Deoxyguanosine triphosphate (dGTP) <sup>[a]</sup>	0.53 ± 0.02	0.33 ± 0.03	-8.4 ± 0.1	-15.4 ± 0.6	-24.8 ± 2.2	-7.01 ± 0.62	56.9 ± 0.3
Differences			ΔΔG (kcal/mol)	ΔΔH (kcal/mol)	ΔΔS (cal/mol/°C)	Δ(T•ΔS) (kcal/mol) <sup>[c]</sup>	ΔT <sub>sq</sub> (°C)
dTTP – dUTP			-1.1	+0.3	+5.0	+1.42	3.3
7Me-GTP – GTP			0	+0.3	+1.2	+0.34	3.7
2S-dTTP – dTTP			0	-0.2	-1.0	-0.28	-0.2
2'OMe-TTP – dTTP			-0.2	-4.5	-15.0	-4.24	0.2
UTP – dUTP			-0.1	-3.8	-13.3	-3.76	0.3
ATP – dATP			-0.5	-3.3	-9.8	-2.77	0.1
GTP – dGTP			-0.3	-2.0	-5.9	-1.68	0.8

<sup>[a]</sup> Values represent the averages of four experiments for ATP, 2'-O-Methyl-5-Methyl-UTP, dTTP, and dUTP, three experiments for 2-Thio-dTTP, and two experiments for 7-Methyl-GTP, dATP, GTP, dGTP and UTP.

<sup>[b]</sup> The average binding stoichiometry of the compounds was approximately 0.5, which presumably reflects ~50% of the protein being in an aggregated and therefore binding-incompetent state as a result of quantitatively removing ATP prior to titration. Residual ATP concentration was confirmed by HPLC to be no more than 1 μM. Protein concentrations ranged from 23 - 49 μM. See Experimental Procedures for further explanation.

<sup>[c]</sup> Calculated using 283 °K, the temperature used for the ITC measurements.

Table S2. Data collection and refinement statistics for nucleotide-bound F508-hNBD1 $\Delta$ RI crystal structures. <sup>a</sup>

Ligand name	ATP	dTTP	dUTP	7Me-GTP	GTP	CTP	UTP	TTP	dATP	dGTP	dCTP
PDB ID	5TF7	5TF8	5TFA	5TFB	5TFC	5TFD	5TFF	5TFG	5TGK	5TFI	5TFJ
Wavelength (Å)	1.18076	0.97907	0.97915	0.97915	1.18076	1.18076	1.18076	1.18076	1.18076	1.18076	1.18076
Resolution range (Å)	50.00-1.93 (1.99-1.93)	50.00-1.86 (1.93-1.86)	50.00-1.87 (1.94-1.87)	50.00-1.87 (1.94-1.87)	50.00-1.92 (1.99-1.92)	50.00-1.89 (1.92-1.89)	50.00-1.89 (1.92-1.89)	50.00-1.98 (1.98-1.91)	50.00-1.91 (1.98-1.91)	50.00-1.89 (1.92-1.89)	50.00-1.85 (1.88-1.85)
Space group	<i>P</i> <sub>4</sub> <sub>3</sub>										
Cell dimensions											
<i>a</i> (Å)/ $\alpha$ (°)	40.29/90	40.19/90	40.12/90	40.29/90	40.13/90	40.18/90	40.18/90	40.15/90	40.16/90	40.17/90	40.14/90
<i>b</i> (Å)/ $\beta$ (°)	40.29/90	40.19/90	40.12/90	40.29/90	40.13/90	40.18/90	40.18/90	40.15/90	40.16/90	40.17/90	40.14/90
<i>c</i> (Å)/ $\gamma$ (°)	141.17/90	141.75/90	141.59/90	141.64/90	141.70/90	141.72/90	141.79/90	141.79/90	141.78/90	141.75/90	141.74/90
Total reflections	123451	73336	108441	141496	130352	136965	137150	131820	131970	136724	145829
Unique reflections	16720 (1640)	18715 (1875)	18365 (1831)	18615 (1874)	17056 (1711)	17893 (1786)	17909 (1794)	16965 (1625)	17270 (1690)	17866 (1784)	19076 (1929)
Multiplicity	7.4	3.9	5.9	7.6	7.6	7.6	7.6	7.8	7.6	7.6	7.6
Completeness (%)	99.4 (98.0)	99.5 (99.0)	99.4 (99.0)	100.0 (100.0)	100.0 (100.0)	100.0 (100.0)	100.0 (100)	97.7 (96.3)	99.9 (99.8)	100.0 (100.0)	100.0 (100.0)
<i>I</i> / $\sigma$	47.6 (13.0)	31.9 (8.4)	34.6 (8.6)	46.8 (12.4)	36.2 (8.3)	57.0 (6.7)	44.4 (11.5)	60.5 (21.2)	49.2 (13.6)	54.0 (24.2)	36.0 (11.0)
Wilson B-factor	19.10	15.97	15.30	15.67	17.15	16.30	16.29	19.04	18.89	15.46	15.81
<i>R</i> <sub>sym</sub>	0.053 (0.143)	0.061 (0.188)	0.102 (0.257)	0.077 (0.177)	0.066 (0.270)	0.095 (0.289)	0.058 (0.166)	0.042 (0.123)	0.06 (0.233)	0.036 (0.083)	0.115 (0.166)
Refinement											
Reflections used in refinement	16716 (1640)	18715 (1875)	18365 (1831)	18614 (1874)	17053 (1711)	17893 (1786)	17907 (1794)	16962 (1625)	17270 (1691)	17865 (1784)	19073 (1929)
Reflections used for R-free	1681 (165)	1866 (188)	1495 (147)	1506 (156)	1689 (166)	1794 (177)	1804 (179)	1714 (163)	1718 (170)	1802 (178)	1883 (190)
<i>R</i> <sub>work</sub>	0.1569 (0.1523)	0.1530 (0.1732)	0.1587 (0.1673)	0.1513 (0.1487)	0.1548 (0.1562)	0.1613 (0.1602)	0.1595 (0.1631)	0.1564 (0.1609)	0.1556 (0.1606)	0.1606 (0.1552)	0.1621 (0.1657)
<i>R</i> <sub>free</sub>	0.1996 (0.2056)	0.1870 (0.2239)	0.1962 (0.2177)	0.1991 (0.2225)	0.2017 (0.2179)	0.1956 (0.1976)	0.1899 (0.2061)	0.1827 (0.2114)	0.1965 (0.2245)	0.2013 (0.2093)	0.1854 (0.2052)
Number of non-hydrogen atoms	1870	1956	1955	1890	1922	1890	1878	1878	1841	1888	1877
<i>macromolecules</i>	1670	1718	1711	1647	1704	1652	1652	1657	1636	1664	1652
<i>ligands</i>	32	30	29	34	33	30	30	31	31	32	29
Protein residues	217	218	218	216	219	216	216	216	217	216	216
RMS(bonds)	0.011	0.007	0.008	0.018	0.007	0.008	0.007	0.009	0.007	0.007	0.007
RMS(angles)	1.00	0.91	0.95	1.59	0.91	0.93	0.81	1.11	0.91	0.92	0.93
Ramachandran favored (%)	99.1	98.6	98	98.1	99	98.1	98.6	99	98.1	98.6	98.6
Ramachandran allowed (%)	0.9	1.4	2.3	1.9	1.4	1.9	1.4	0.94	1.9	1.4	1.4
Ramachandran outliers (%)	0	0	0	0	0	0	0	0	0	0	0
Rotamer outliers (%)	0	0	0	0	0.54	0	0	0	0	0	0
Clashscore	1.77	3.43	4.31	1.81	3.76	4.20	2.10	5.39	2.41	2.96	3.30
Average B-factor	22.43	19.58	19.43	18.40	20.54	19.19	18.17	22.01	20.97	17.91	18.61
<i>macromolecules</i>	21.68	18.33	17.88	16.87	19.34	17.97	16.97	20.87	20.07	16.71	17.48
<i>ligands</i>	25.81	20.84	23.69	20.57	27.70	21.03	22.13	22.73	24.32	22.59	19.98
<i>solvent</i>	29.16	29.77	31.19	30.09	30.31	28.64	27.67	31.77	28.99	27.51	27.94

<sup>a</sup> Data-collection and refinement statistics were calculated using *HKL* (2) and *PHENIX* (3), respectively. Statistics for the highest-resolution shell are shown in parentheses.

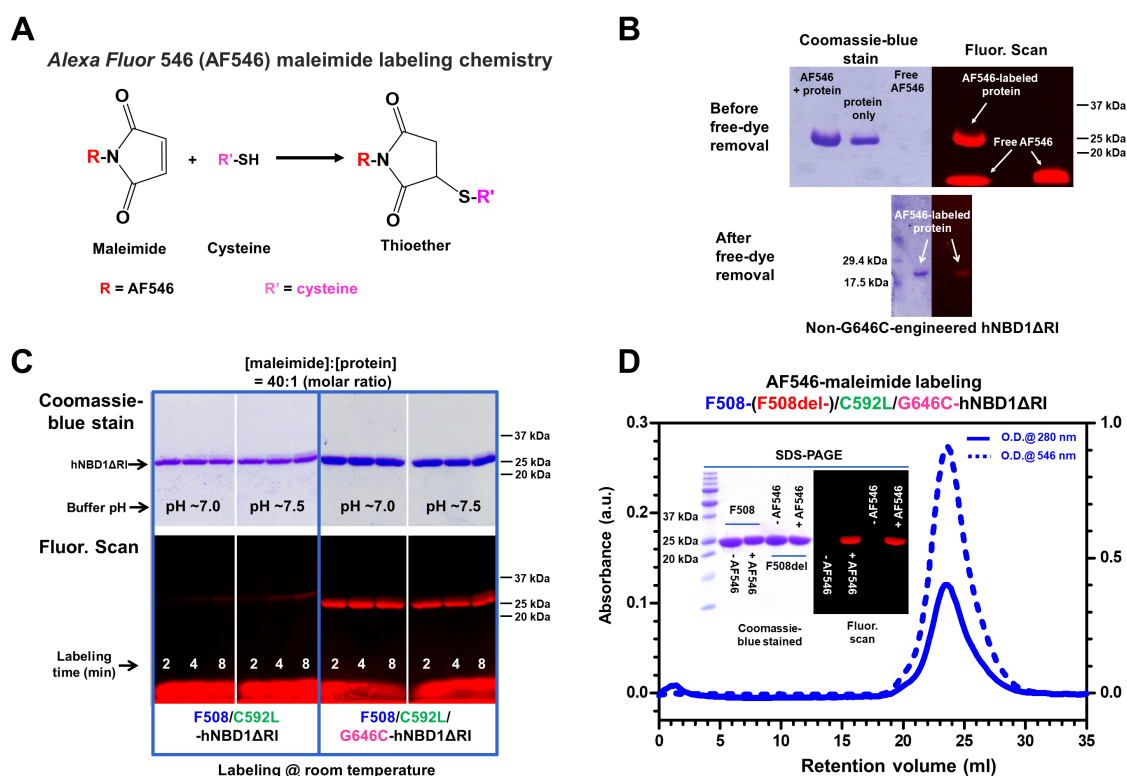


**Figure S1. Selective fluorescent labeling of engineered hNBD1 domains using maleimide reagents.** (A) Chemical schematic showing the labeling reaction, with  $R'$  representing a cysteine residue in the protein domain. (B) Labeling of the F508-hNBD1 $\Delta$ RI base construct at 50  $\mu$ M (1.25 mg/mL) with 500  $\mu$ M AlexaFluor 546 (AF546) maleimide overnight at 4  $^{\circ}$ C in Standard Stabilizing Buffer (SSB). Following quenching of unreacted maleimide with 280 mM  $\beta$ -mercaptoethanol ( $\beta$ ME), the reaction was analyzed by SDS-PAGE either before (top) or after (bottom) buffer exchange to remove unreacted dye. The gel was stained with Coomassie Blue to detect total protein (left panels with blue bands) and scanned for AF546 emission (right panels with red bands). The protein construct, which retains all four endogenous cysteine residues in native hNBD1, is strongly labeled by AF546 but aggregates and is lost during subsequent buffer exchange. (C) Labeling of 20  $\mu$ M (0.50 mg/mL) F508-C592L-hNBD1 $\Delta$ RI (left) or F508-C592L/G646C-hNBD1 $\Delta$ RI (right) with 800  $\mu$ M fluorescein maleimide for 2, 4, or 8 minutes (white labels) at room temperature in SSB at pH 7.0 (panels on the left in each set) or pH 7.5 (panels on the right in each set). Reactions were stopped by mixing with SDS Sample Buffer containing 5 mM  $\beta$ ME and analyzed on SDS-PAGE gels that were stained with Coomassie Blue (top) and scanned for fluorescein emission (bottom). (D) Labeling and purification of C592L/G646C-hNBD1 $\Delta$ RI constructs harboring the wild-type F508 residue or the F508del mutation. Reactions containing 20  $\mu$ M (0.50 mg/mL) protein and 200  $\mu$ M AF546 maleimide were incubated for 5 minutes at room temperature and then five minutes on ice (F508) or for 5 minutes on ice (F508del) in SSB at pH 7.5 prior to quenching with 280 mM  $\beta$ ME. Free dye was removed using a PD10 desalting column before gel filtration on Superdex 200 in the same buffer. The chromatogram shows the absorbance at 280 nm (solid line) and 546 nm (dotted line) during gel filtration of the F508 construct. The fluorescently labeled proteins and unlabeled control samples were analyzed

on a 12.5% SDS-PAGE gel, which was stained with Coomassie Blue (left side of inset) after scanned for AF546 emission (right side of inset).

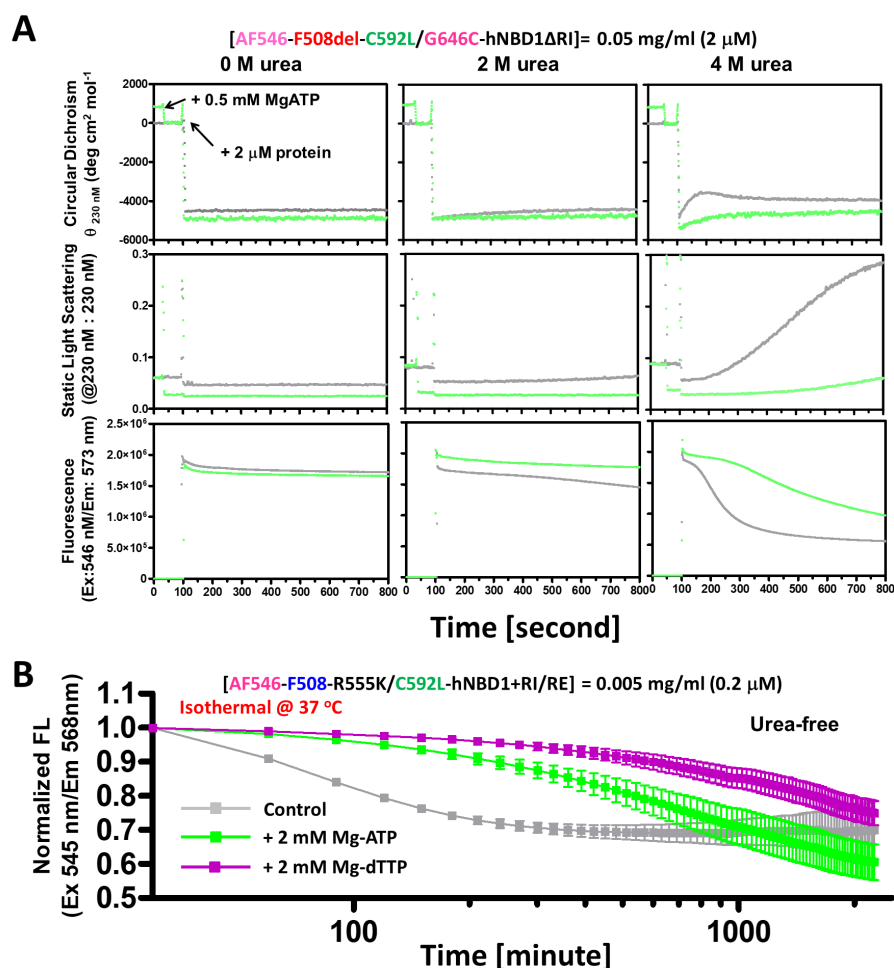


**Figure S2. Isothermal fluorescence self-quenching (iFSQ) assays for hNBD1 stability in the presence of urea and at elevated temperature.** (A) Triple detection experiment using circular dichroism (CD – top row), static light-scattering (SLS – middle row), and visible fluorescence emission intensity at 573 nm (bottom row) to monitor the kinetics of unfolding and aggregation of AF546-labeled F508del-C592L/G646C-hNBD1ΔRI in urea solutions. Signals were monitored as a function of time after adding the protein at 100 seconds to SSB at 25 °C containing 0 M (left), 2 M (middle), or 4 M (right) urea in the presence of 30 μM (gray) or 530 μM (light-green) Mg-ATP. The SLS traces show that the protein aggregates slowly in 2 M urea and more rapidly in 4 M urea and that the rate of aggregation in both environments is reduced when the concentration of Mg-ATP is increased. The visible fluorescence emission intensity at 573 nm decreases due to self-quenching of the AF546 fluorescence upon protein aggregation. This isothermal fluorescence self-quenching (iFSQ) signal provides the most sensitive monitor of the aggregation process. (B) The use of iFSQ to monitor the kinetics of unfolding and aggregation of AF546-labeled F508-C592L/R555K-hNBD1+RI/RE in SSB at 37 °C. Assays were conducted using 0.005 mg/mL (~0.2 μM) protein in the presence of 3 μM Mg-ATP (gray), 2.003 mM Mg-ATP (green), or 3 μM Mg-ATP and 2.0 mM Mg-dTTP (magenta). The iFSQ assays provide a highly sensitive monitor for protein aggregation that qualitatively demonstrates stronger stabilization of the domain by dTTP than ATP.

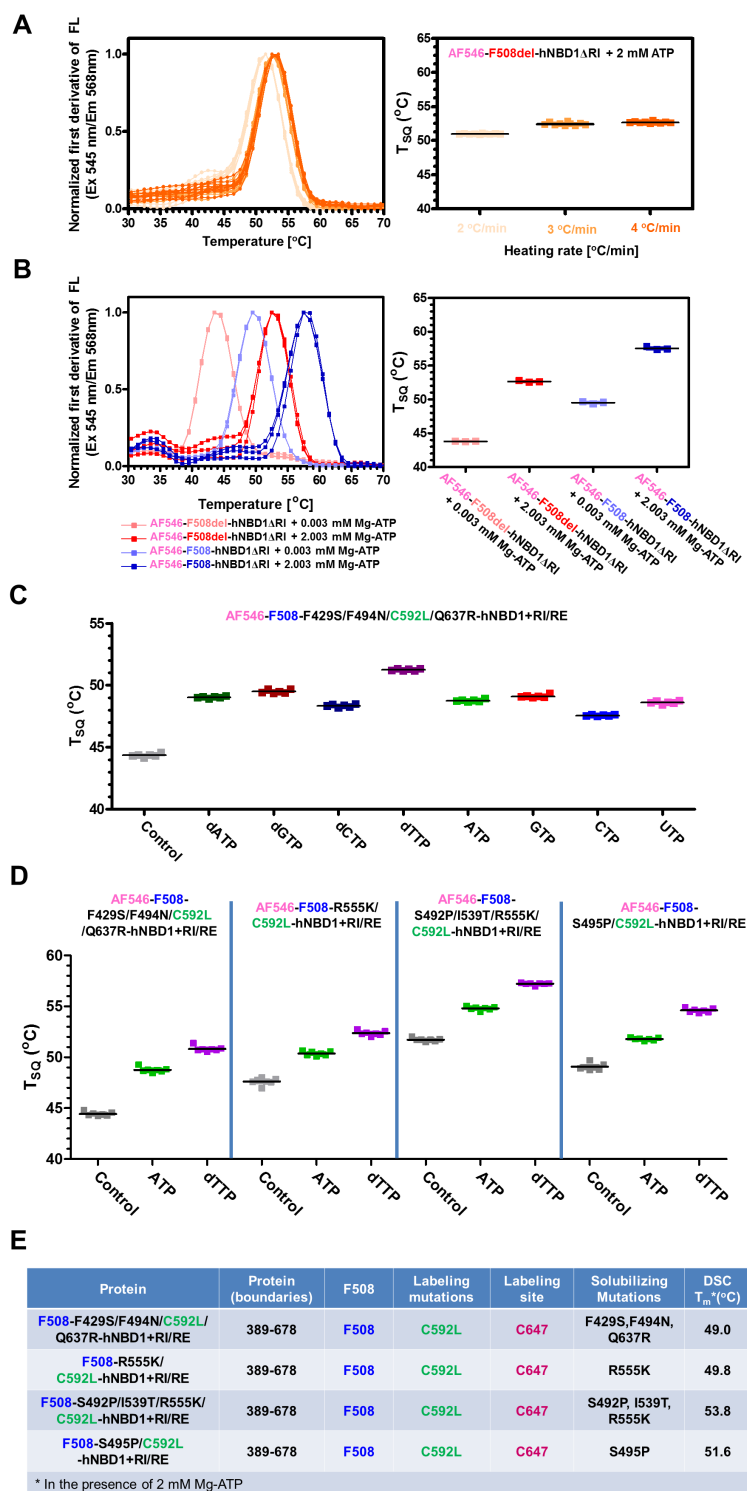


**Figure S3. Implementation of the tFSQ assay in diverse AF546-labeled hNBD1 constructs.** (A) Results from tFSQ assays conducted as in Fig 3B-C on AF546-labeled F508del-C592L/G646C-hNBD1 $\Delta$ RI) in the presence of 2mM ATP at three different heating scan rates from 2-4°C/min. The  $T_{SQ}$  increases from  $51.0 \pm 0.1$  °C at 2 °C/min to  $52.7 \pm 0.1$  °C at 4 °C/min. (B) Results from

## Supplementary Figure S3 (cont.)

tFSQ assays conducted as in **Fig 3B-C** on matched AF546-labeled hNBD1 $\Delta$ RI constructs harboring (F508del-C592L/G646C-hNBD1 $\Delta$ RI) or not harboring (F508-C592L/G646C-hNBD1 $\Delta$ RI) the F508del mutation. The left panel shows the first derivative of fluorescence emission intensity at 586 nm (top) in three replicate assays conducted on each protein construct in SSB in the presence of 3  $\mu$ M or 2.003 mM Mg-ATP, and the right panel shows the derived  $T_{SQ}$  values. These assays were all conducted simultaneously in a single microtiter plate. **(C-E)** Results from equivalent tFSQ assays conducted in the presence of a 2 mM concentration of the Mg<sup>++</sup> complex of the indicated nucleotide on a series of AF546-labeled full-length hNBD1 constructs that contain both the Regulatory Insertion (RI – residues 405-436 in native hCFTR) and Regulatory Extension (RE – residues 647-678 in native hCFTR). The string “+RI/RE” in the construct names denotes the presence of these two segments, neither of which is present in the hNBD1 $\Delta$ RI construct (4-7) used for most experiments in this paper. These hNBD1 constructs contain different stabilizing mutations (4,8,9) that are indicated at the top of the graphs in panels **C-D** and in the penultimate column on the right in table in panel **E**. The presence of the RI segment is sufficiently destabilizing (6) that full-length hNBD1 constructs cannot be purified in monodisperse form in the absence of stabilizing mutations (4,8,9). The full-length hNBD1 constructs characterized here all retain the native F508 residue and harbor the C592L mutation that prevents fluorescent labeling at this site. These constructs are labeled by AF546-maleimide at residue C647, an endogenous cysteine at the N-terminus of the RE segment in hCFTR. The control assays contained 3  $\mu$ M Mg-ATP, which comes from the protein storage buffer and is present in all samples in addition to any added nucleotide. The tFSQ assay data presented here demonstrate that, in all hNBD1 constructs tested, Mg-dTTP produces a consistent increase in  $T_{SQ}$  relative to Mg-ATP, indicating that dTTP has an equivalent stabilizing effect on a wide variety of hNBD1 constructs harboring different sequence variations.

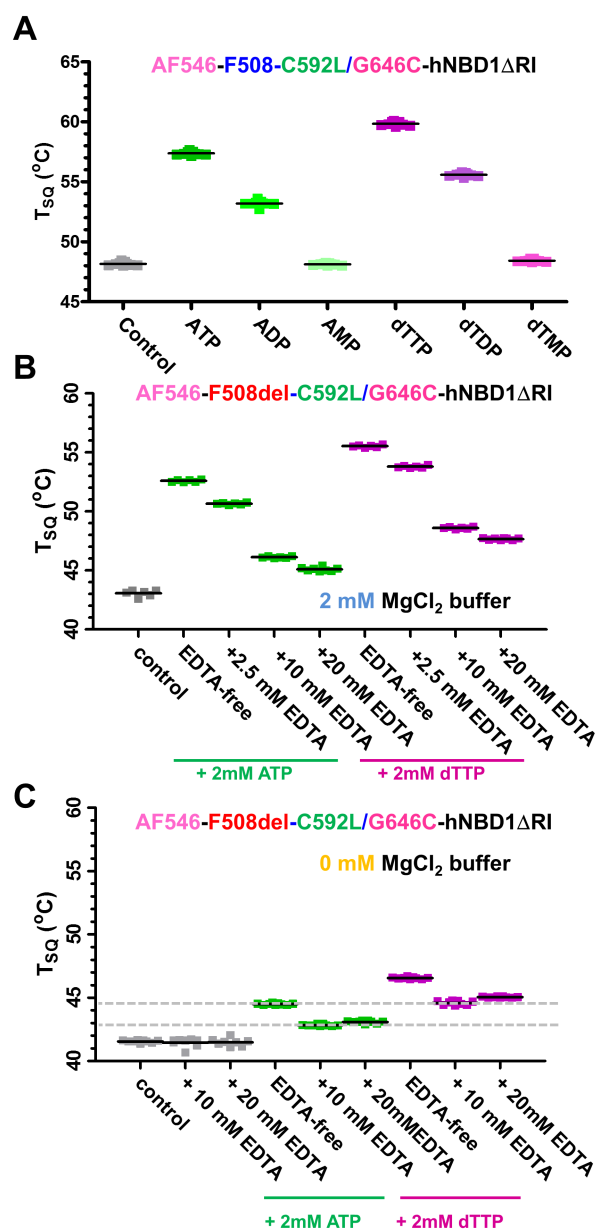


**Figure S4. Dissection of the contributions of the phosphate groups and the  $Mg^{++}$  cofactor to nucleotide stabilization of hNBD1 $\Delta$ RI.** Data from samples containing adenine or thymine nucleotides are shown in shades of green or magenta, respectively, and data from control samples are shown in gray. All assays were conducted in microtiter plates as described in **Fig 3B-C**. **(A)** T<sub>SQ</sub> values from nine replicate tFSQ assays conducted on AF546-labeled F508-C592L/G646C-hNBD1 $\Delta$ RI in the presence of a 2 mM concentration of the  $Mg^{++}$  complex of the indicated nucleotide in SSB. Different shades of each green and magenta are used to represent data from monophosphate (lightest shades), diphosphate (intermediate shades), and triphosphate (darkest shades) species. The nucleotide monophosphates (AMP and dTMP) do not produce detectable stabilization of the protein domain. The nucleotide triphosphates (ATP and dTTP) both produce stronger stabilization than the corresponding diphosphates (ADP and dTDP). For both the

## Supplementary Figure S4 (cont.)

diphosphate and triphosphates, the thymine nucleotides produce stronger stabilization than the corresponding adenine nucleotides. The control assays for this experiment contained 3  $\mu\text{M}$  Mg-ATP, which came from the protein storage buffer and was present in all samples in addition to any added nucleotide. **(B-C)**  $T_{\text{SQ}}$  values from five (panel **B**) or eight (panel **C**) replicate tFSQ assays conducted on AF546-labeled F508del-C592L/G646C-hNBD1 $\Delta$ RI in the presence of different concentrations of  $\text{Mg}^{++}$  and EDTA. The increase in  $T_{\text{SQ}}$  in the  $\text{Mg}^{++}$ -free buffer upon addition of 2 mM ATP or dTTP together with 10 mM or 20 mM EDTA (panel **C**) demonstrates that these nucleotides both bind to the domain and stabilize it significantly in the absence of  $\text{Mg}^{++}$ , even though the  $\text{Mg}^{++}$  cofactor promotes substantially tighter binding and stronger thermal stabilization of hNBD1. In the absence of  $\text{Mg}^{++}$ , the nucleotides presumably bind to hNBD1 with a  $\text{Na}^+$  cofactor, as previously demonstrated for the bacterial homolog MJ0796 (PDB id 1L2T) (10). The failure to see a reduction in the thermal stabilization of hNBD1 by ATP or dTTP when EDTA concentration is increased from 10 mM to 20 mM, which cuts the residual free  $\text{Mg}^{++}$  concentration in half, strongly supports binding of these nucleotides in the absence of a  $\text{Mg}^{++}$  cofactor. Notably, dTTP stabilizes hNBD1 more strongly than ATP either in the presence (**Fig 4A**) or absence (panel **C**) of  $\text{Mg}^{++}$ . These assays were conducted in SSB containing either a reduced 2 mM concentration of  $\text{MgCl}_2$  (panel **B**) or no  $\text{MgCl}_2$  (panel **C**). The control assays contained 4  $\mu\text{M}$  ATP and 8  $\mu\text{M}$   $\text{Mg}^{++}$ , which came from the protein storage buffer and were present in all samples in addition to any added nucleotide or divalent cation

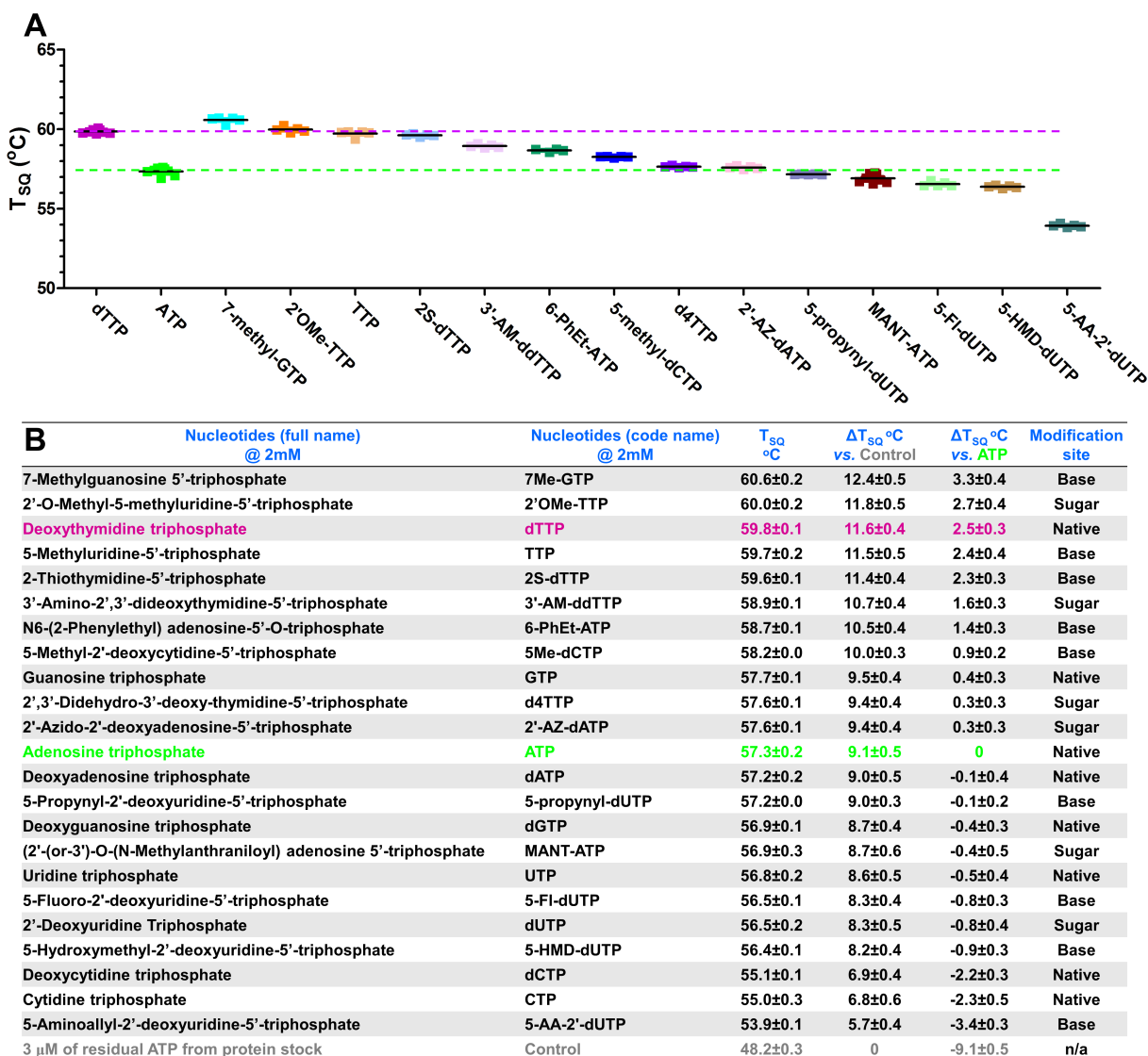


**Figure S5. More extensive structure–activity relationship for stabilization of hNBD1 by nucleotide analogs established using the *tFSQ* assay.**  $T_{SQ}$  values are shown from replicate assays conducted on AF546-labeled F508-C592L/G646C-hNBD1 $\Delta$ RI in the presence of a 2 mM concentration of the  $Mg^{++}$  complex of the indicated nucleotide. Assays were conducted in SSB using heat rate of 3 °/min in a microtiter plate as in Fig 3B-C. Compounds other than dTTP (magenta) and ATP (green) are ordered from the highest to the lowest observed  $T_{SQ}$  going left to right. The nucleotides 7Me-GTP, 2'OMe-TTP, TTP, and 2S-TTP yield similar  $T_{SQ}$  values to dTTP. Eight replicate assays were performed for ATP and dTTP, and five replicate assays were performed for all other nucleotides.

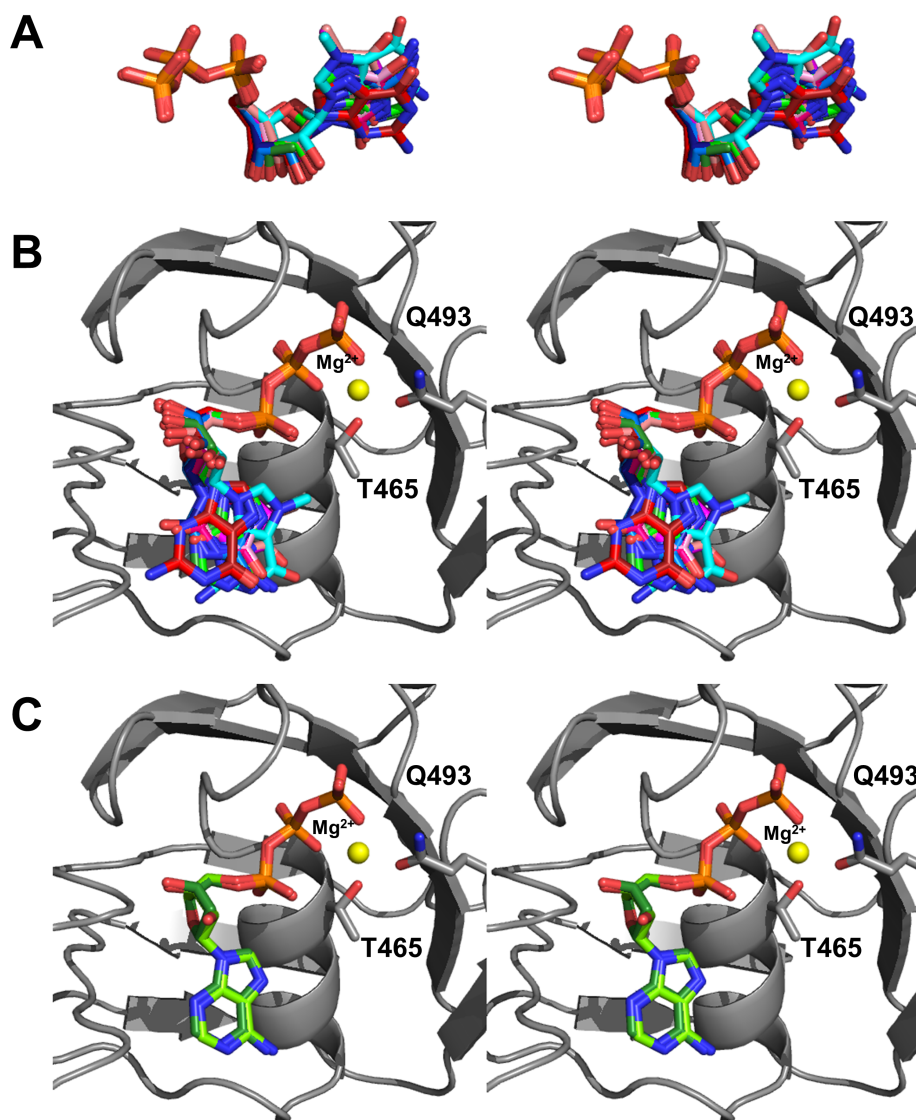
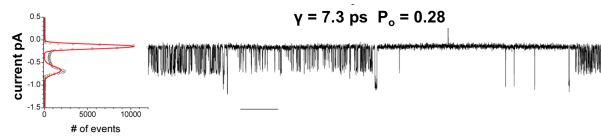
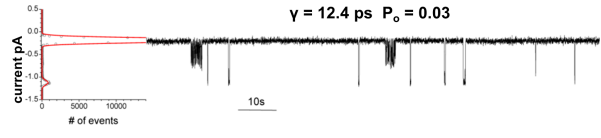
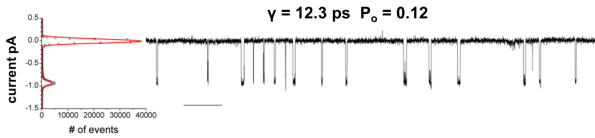


**Figure S6. Stereo views of crystal structures of nucleotide analogs bound to F508-hNBDARI.** (A) Ball-and-stick representations of the nucleotide analogs in all structures in **Table S1**, aligned based on least-squares superposition of all C $\alpha$  atoms in the protein domain. The carbon atoms in each nucleotide are colored the same as the corresponding T<sub>SQ</sub> data in **Figs 4A-B** (green for ATP, dark green for dATP, maroon for GTP, red for dGTP, cyan for 7Me-GTP, blue for CTP, dark blue for dCTP, light magenta for UTP, pink for dUTP, magenta for dTTP, and salmon for TTP). Oxygen, nitrogen, and phosphorous atoms are colored red, blue, and orange, respectively. (B) Alternative view of the same nucleotide analog structures with the protein backbone and residues Q493 and T465 from the dTTP structure (PDB id 5TF8) shown in gray and the Mg<sup>2+</sup> cofactor bound to the nucleotide in that structure shown as an orange sphere. (C) Equivalent view showing just the ATP and dATP structures from panel **B** (PDB ids 5TF7 and 5TGK, respectively).

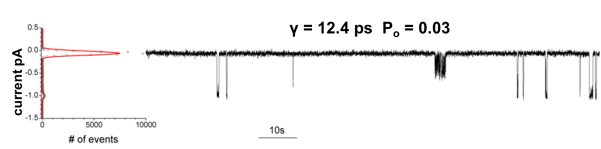
## 5Me-dCTP



## 2S-dTTP



## 2'OMe-dTTP



WT-hCFTR @ 30 °C

rF508del-hCFTR @ 30 °C

**Figure S7. Temperature-dependent single-channels electrophysiology analyses of full-length hCFTR interacting with three additional nucleotide analogs.** Single-channel electrophysiology measurements conducted at 30 °C on WT-hCFTR (left) or rF508del-hCFTR (11) (right) reconstituted into black lipid membranes(12,13). Measurements were conducted in the presence of 1 mM 5Me-dCTP (top), 2S-dTTP (middle), or 2'-OMe-TTP (bottom). Electrical current is indicated in picoamps (pA), time is indicated in seconds (s), and conductivity is indicated in picosiemens (pS). The plot on the left in each panel shows a histogram with the observed current on the ordinate, which was used to calculate the open probability of the channel ( $P_o$ ).

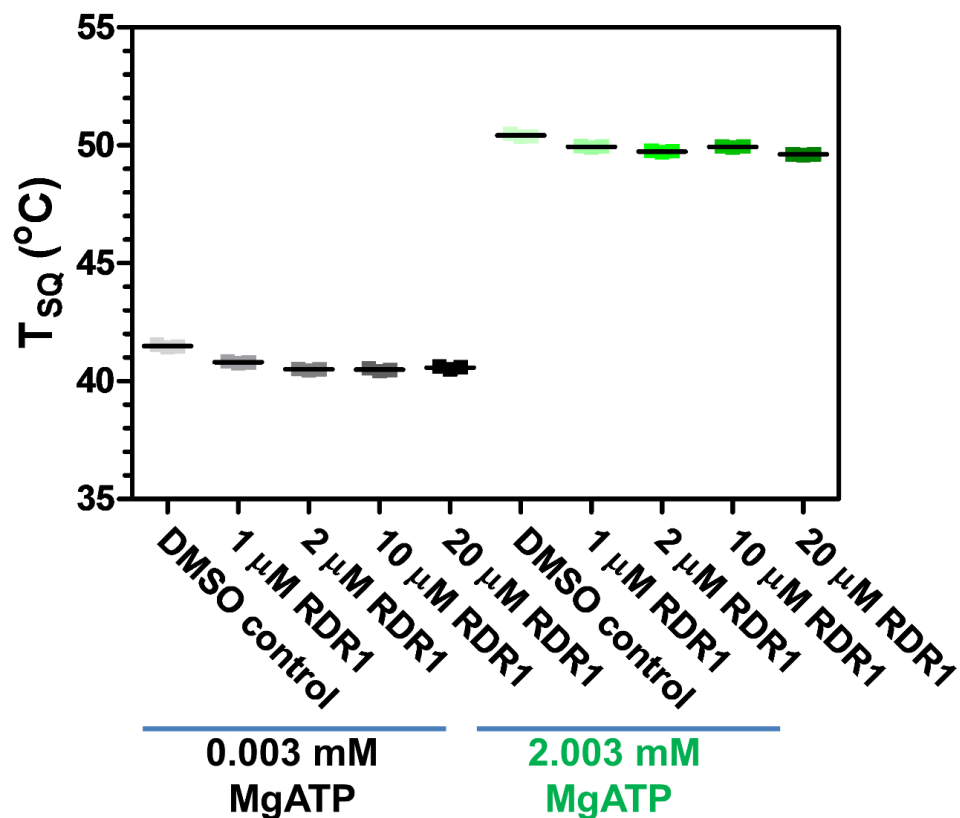


**Figure S8. Results from *tFSQ* assays on AF546-labeled F508del-hNBD1 $\Delta$ RI in the presence of the compound RDR1.**  $T_{SQ}$  values are shown from assays conducted in the presence of the indicated concentration of RDR1 and either 3  $\mu$ M (left) or 2.003 mM (right) Mg-ATP. The compound RDR1, which has strong absorbance peaks at 362 nm and 580 nm, was previously demonstrated to increase the apparent unfolding temperature of hNBD1 (14,15) in differential scanning fluorimetry assays conducted using Sypro Orange (16)

## Supplementary References

1. Zhou, Z., Wang, X., Li, M., Sohma, Y., Zou, X., and Hwang, T. C. (2005) High affinity ATP/ADP analogues as new tools for studying CFTR gating. *J Physiol* **569**, 447-457
2. Otwinowski, Z., and Minor, W. (1997) Processing of X-ray diffraction data collected in oscillation mode. *Method Enzymol* **276**, 307-326
3. Adams, P. D., Afonine, P. V., Bunkoczi, G., Chen, V. B., Davis, I. W., Echols, N., Headd, J. J., Hung, L. W., Kapral, G. J., Grosse-Kunstleve, R. W., McCoy, A. J., Moriarty, N. W., Oeffner, R., Read, R. J., Richardson, D. C., Richardson, J. S., Terwilliger, T. C., and Zwart, P. H. (2010) PHENIX: a comprehensive Python-based system for macromolecular structure solution. *Acta Crystallogr D Biol Crystallogr* **66**, 213-221
4. Lewis, H. A., Zhao, X., Wang, C., Sauder, J. M., Rooney, I., Noland, B. W., Lorimer, D., Kearins, M. C., Connors, K., Condon, B., Maloney, P. C., Guggino, W. B., Hunt, J. F., and Emtage, S. (2005) Impact of the deltaF508 mutation in first nucleotide-binding domain of human cystic fibrosis transmembrane conductance regulator on domain folding and structure. *J Biol Chem* **280**, 1346-1353
5. Wang, C., Protasevich, I., Yang, Z., Seehausen, D., Skalak, T., Zhao, X., Atwell, S., Spencer Emtage, J., Wetmore, D. R., Brouillette, C. G., and Hunt, J. F. (2010) Integrated biophysical studies implicate partial unfolding of NBD1 of CFTR in the molecular pathogenesis of F508del cystic fibrosis. *Protein Sci* **19**, 1932-1947
6. Atwell, S., Brouillette, C. G., Connors, K., Emtage, S., Gheyi, T., Guggino, W. B., Hendle, J., Hunt, J. F., Lewis, H. A., Lu, F., Protasevich, I., Rodgers, L. A., Romero, R., Wasserman, S. R., Weber, P. C., Wetmore, D., Zhang, F. F., and Zhao, X. (2010) Structures of a minimal human CFTR first nucleotide-binding domain as a monomer, head-to-tail homodimer, and pathogenic mutant. *Protein Eng Des Sel* **23**, 375-384
7. Protasevich, I., Yang, Z., Wang, C., Atwell, S., Zhao, X., Emtage, S., Wetmore, D., Hunt, J. F., and Brouillette, C. G. (2010) Thermal unfolding studies show the disease causing F508del mutation in CFTR thermodynamically destabilizes nucleotide-binding domain 1. *Protein Sci* **19**, 1917-1931
8. Lewis, H. A., Wang, C., Zhao, X., Hamuro, Y., Connors, K., Kearins, M. C., Lu, F., Sauder, J. M., Molnar, K. S., Coales, S. J., Maloney, P. C., Guggino, W. B., Wetmore, D. R., Weber, P. C., and Hunt, J. F. (2010) Structure and dynamics of NBD1 from CFTR characterized using crystallography and hydrogen/deuterium exchange mass spectrometry. *J Mol Biol* **396**, 406-430
9. Aleksandrov, A. A., Kota, P., Cui, L., Jensen, T., Alekseev, A. E., Reyes, S., He, L., Gentzsch, M., Aleksandrov, L. A., Dokholyan, N. V., and Riordan, J. R. (2012) Allosteric modulation balances thermodynamic stability and restores function of DeltaF508 CFTR. *J Mol Biol* **419**, 41-60
10. Smith, P. C., Karpowich, N., Millen, L., Moody, J. E., Rosen, J., Thomas, P. J., and Hunt, J. F. (2002) ATP binding to the motor domain from an ABC transporter drives formation of a nucleotide sandwich dimer. *Mol Cell* **10**, 139-149

11. Boyle, M. P., Bell, S. C., Konstan, M. W., McColley, S. A., Rowe, S. M., Rietschel, E., Huang, X., Waltz, D., Patel, N. R., Rodman, D., and group, V. X. s. (2014) A CFTR corrector (lumacaftor) and a CFTR potentiator (ivacaftor) for treatment of patients with cystic fibrosis who have a phe508del CFTR mutation: a phase 2 randomised controlled trial. *Lancet Respir Med* **2**, 527-538
12. He, L., Aleksandrov, A. A., An, J., Cui, L., Yang, Z., Brouillette, C. G., and Riordan, J. R. (2015) Restoration of NBD1 thermal stability is necessary and sufficient to correct F508 CFTR folding and assembly. *J Mol Biol* **427**, 106-120
13. Aleksandrov, L. A., Jensen, T. J., Cui, L., Kousouros, J. N., He, L., Aleksandrov, A. A., and Riordan, J. R. (2015) Thermal stability of purified and reconstituted CFTR in a locked open channel conformation. *Protein Expr Purif* **116**, 159-166
14. Sampson, H. M., Lam, H., Chen, P. C., Zhang, D., Mottillo, C., Mirza, M., Qasim, K., Shrier, A., Shyng, S. L., Hanrahan, J. W., and Thomas, D. Y. (2013) Compounds that correct F508del-CFTR trafficking can also correct other protein trafficking diseases: an in vitro study using cell lines. *Orphanet J Rare Dis* **8**, 11
15. Sampson, H. M., Robert, R., Liao, J., Matthes, E., Carlile, G. W., Hanrahan, J. W., and Thomas, D. Y. (2011) Identification of a NBD1-binding pharmacological chaperone that corrects the trafficking defect of F508del-CFTR. *Chem Biol* **18**, 231-242
16. Lo, M. C., Aulabaugh, A., Jin, G., Cowling, R., Bard, J., Malamas, M., and Ellestad, G. (2004) Evaluation of fluorescence-based thermal shift assays for hit identification in drug discovery. *Anal Biochem* **332**, 153-159